

# Closed-shell polycyclic aromatic hydrocarbon cations: a new category of interstellar polycyclic aromatic hydrocarbons

Douglas M. Hudgins, Charles W. Bauschlicher, Jr \*, Louis J. Allamandola

*NASA Ames Research Center, MS 230-3, Moffett Field, CA 94035, USA*

Received 11 July 2000; received in revised form 14 September 2000; accepted 18 September 2000

## Abstract

Density functional theory has been employed to calculate the harmonic frequencies and intensities of a range of polycyclic aromatic hydrocarbon (PAH) cations that explore both size and electronic structure effects on the infrared spectroscopic properties of these species. The sample extends the size range of PAH species considered to more than 50 carbon atoms and includes several representatives from each of two heretofore unexplored categories of PAH cations: (1) fully benzenoid PAH cations whose carbon skeleton is composed of an odd number of carbon atoms ( $C_{\text{odd}}$  PAHs); and (2) protonated PAH cations (HPAH<sup>+</sup>). Unlike the radical electronic structures of the PAH cations that have been the subject of previous theoretical and experimental work, the species in these two classes have a ‘closed’-shell electronic configuration. The calculated spectra of circumcoronene,  $C_{54}H_{18}$ , in both neutral and (radical) cationic form are also reported and compared with those of the other species. Overall, the  $C_{\text{odd}}$  PAHs spectra are dominated by strong CC stretching modes near  $1600\text{ cm}^{-1}$  and display spectra that are remarkably insensitive to molecular size. The HPAH<sup>+</sup> species evince a more complex spectrum consistent with the added contributions of aliphatic modes and their generally lower symmetry. Finally, for both classes of closed-shell cations, the intensity of the aromatic CH stretching modes is found to increase with molecular size far out of proportion with the number of CH groups, approaching a value more typical of neutral PAHs for the largest species studied. © 2001 Published by Elsevier Science B.V.

*Keywords:* Infrared spectroscopy; Polycyclic aromatic hydrocarbon; Harmonic frequencies and intensities; Interstellar molecules

## 1. Introduction

The discovery of an unexpected infrared emission feature from two planetary nebulae by Gillett, Forrest, and Merrill in 1973 marked the

beginning of an exciting chapter of modern astrophysics [1]. Gillett et al. recognized that this band near  $885\text{ cm}^{-1}$  ( $11.3\text{ }\mu\text{m}$ ) was associated with interstellar dust, and that its identification could give important insight into dust formation and evolution through the latter stages of the stellar life cycle. Moreover, this feature could not be associated with graphite grains, long thought to be produced in intense circumstellar outflows

\* Corresponding author. Tel.: +1-650-6046231; Fax: +1-650-6045244.

*E-mail address:* bauschli@pegasus.arc.nasa.gov (C.W. Bauschlicher, Jr).

from late-type, carbon-rich stars. Subsequent pioneering observations showed this was just one part of a now well-known spectrum of features emitted from a wide variety of very different astronomical objects (for example, see Refs. [2–5]). This spectrum is characterized by dominant features near 3030, 1610, 1280, 1150, and 890  $\text{cm}^{-1}$  (3.3, 6.2, 7.7, 8.6, and 11.2  $\mu\text{m}$ ) as well as a number of minor bands and underlying continua. The brightest emission is observed from dusty regions exposed to intense ultraviolet radiation. Surprisingly, the age and history of the material seem to be relatively unimportant. Similar emission spectra are observed from objects that span the lifecycle of matter in the interstellar medium (ISM) — from objects only a few thousand years in age (late carbon star ejecta and planetary nebulae shells) to those millions of years in age (H II regions, reflection nebulae, and the diffuse ISM) [6–11]. Understanding the source of this unexpected, yet widespread, phenomenon has become an important problem in astrophysics.

The idea now gaining acceptance, that stochastically heated, gas-phase, polycyclic aromatic hydrocarbons (PAHs) are the band carriers, was first put forth over a decade ago [12,13]. This attribution is based on several pieces of ‘circumstantial’ evidence that point to these species. First, the interstellar emission is non-thermal in nature. The banded (rather than continuous) nature of the spectrum, the typically large feature/continuum ratio, and the close association with ultraviolet radiation all indicate that the emission is due to infrared fluorescence from gas-phase molecules excited by the absorption of single ultraviolet and visible photons rather than thermal emission from a solid material [14]. Second, careful observations of planetary nebulae have established that the fraction of the total infrared energy that is emitted through these features is closely correlated with the amount of available carbon [15], indicating that the gas-phase molecular carriers are carbon rich. Third, since the carbon-rich carriers must survive under remarkably harsh conditions, they must also be extremely stable. Finally, although there are variations among the relative band intensities, the features are correlated [16,17], implying that a single class of chemical

species is responsible. Of course, any proposed carrier must have an IR spectrum consistent with the positions and intensities of these bands. As a molecular class, PAHs readily accommodate all these constraints.

Originally, the principal reason for the assignment to PAHs was the suggestive, but far from perfect, resemblance of the interstellar ‘emission’ spectra to the then-available infrared ‘absorption’ spectra, primarily those of PAH clusters dispersed in KBr pellets or soot particles. Unfortunately, although rich, this spectral database was not adequate to squarely address the astronomical questions since such laboratory conditions strongly perturb the spectrum and are far from those in the interstellar emission zones. Moreover, if PAHs are indeed present in the highly energetic emission zones, they are likely to be ionized [13] and, until recently, there was no spectroscopic data available on the infrared properties of PAH ions. Thus, the spectral database initially available was not sufficient for a critical test of the PAH hypothesis nor, if the hypothesis held up to close scrutiny, was it up to the task of exploiting PAHs as probes of the emission zones. To truly test the PAH hypothesis, special techniques for studying individual PAHs and PAH ions under astrophysically relevant conditions were required.

Motivated in no small part by their emerging interstellar importance, the past decade has seen a renaissance in experimental and theoretical methods aimed at determining the physical [18–20], chemical [21–25], and spectroscopic [26–38] impact of PAHs in the interstellar medium. Particularly relevant to the problem of the interstellar infrared emission, these efforts have produced a large and growing database of the infrared spectroscopic properties of PAHs and PAH ions that are directly relevant to the astrophysical problem [39–55]. These studies have included PAHs in neutral, cationic and anionic forms, and encompass species ranging in size from ten to 32 carbon atoms. Nevertheless, to date, both experimental and theoretical studies in this area have focused primarily on the determination of the spectroscopic properties of the sorts of conventional structures that characterize terrestrially stable, commercially available PAHs. Such PAHs in their

neutral forms (indeed, virtually all stable chemical compounds) have a ‘closed-shell’ electronic structure — one having only paired electrons. This necessarily implies that their daughter cations all have the alternative ‘free-radical’ or ‘open-shell’ electronic structure carrying one unpaired electron. Regardless of their ionization state, due to their incomplete electronic structure, open-shell species are inherently less stable and more reactive than their closed-shell counterparts. Despite the focus on PAH radical cations, PAH cations that have a closed-shell configuration are not unknown. Two classes of these are of particular interest to astrophysics: (1) fully benzenoid PAH cations with an odd number of carbon atoms ( $C_{\text{odd}}$  PAH cations); and (2) protonated PAHs (HPAH<sup>+</sup>). Representative structures from each of these classes are shown

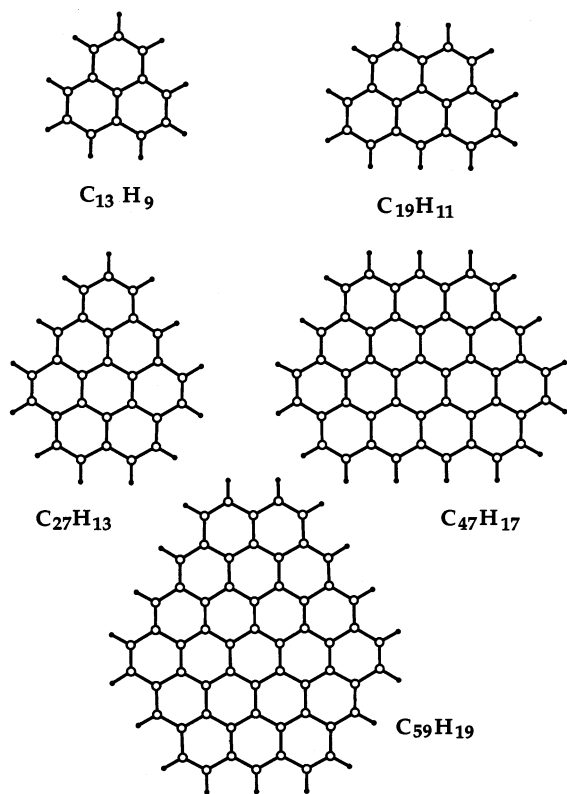


Fig. 1. The structures of the  $C_{\text{odd}}$  PAH cations considered in this work. The species all have a fully benzenoid skeleton composed of an odd number of carbon atoms. The open circles represent carbon atoms.

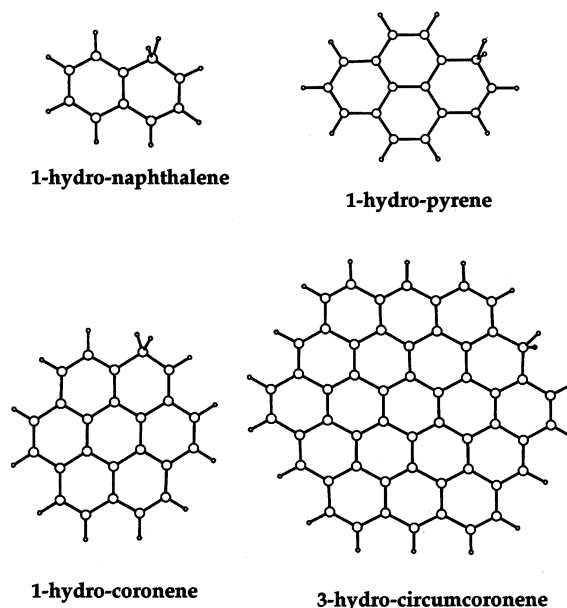


Fig. 2. The structures of the protonated PAH cations, HPAH<sup>+</sup>, considered in this work. Note the aliphatic  $-CH_2-$  groups that replace one aromatic CH in each case. Large circles, carbon atoms; small circles, hydrogen atoms.

in Figs. 1 and 2, respectively. For such closed-shell cations, it is the corresponding neutral species that have the highly reactive radical electron configuration and are not isolatable. The lack of a suitable precursor presents serious practical difficulties that have yet to be overcome with the current experimental techniques. Thus, these classes of closed-shell PAH cations make excellent subjects for a theoretical investigation of their infrared spectroscopic properties.

An additional noteworthy aspect of the computational results presented in the following is the molecular size range of the PAH species that are considered. To date, most studies (experimental and theoretical alike) have focused on PAH molecules containing only up to about 30 carbon atoms. In the theoretical studies, this limitation was imposed largely by the significant amounts of CPU time required for calculations of larger species. However, the latest experimental and theoretical studies suggest that, while molecules containing as few as 20–30 carbon atoms may contribute to the interstellar infrared emission

spectrum, the strongest interstellar emission features in the 1600–1100  $\text{cm}^{-1}$  (6–9  $\mu\text{m}$ ) region are dominated by species comprised of 50–100 carbon atoms [18,35,56]. It is therefore important to the astrophysical problem that studies of PAH cations be extended to species of this size. In this manuscript, with the benefit of several key advances [57] in the calculation of analytic second derivatives (which have been implemented in the GAUSSIAN 98 package of programs), we report computed IR spectra of PAH cations as large as 59 carbon atoms.

This paper is laid out as follows. The computational methods are described in Section 2. In Section 3, the calculated harmonic frequencies and intensities for the two classes of closed-shell PAH cations are presented and discussed according to class, with the  $\text{C}_{\text{odd}}$  PAH cations considered in Section 3.1, and the protonated PAH cations considered in Section 3.2. Finally, the astrophysical implications of the results are considered in Section 4.

## 2. Computational methods

The geometries are optimized, and the harmonic frequencies and infrared intensities are computed using the B3LYP [58] hybrid [59] functional in conjunction with the 4-31G basis sets

[60]. Calibration calculations, which have been carried out for selected systems [36], show that a single scale factor of 0.958 brings the B3LYP harmonic frequencies computed using the 4-31G basis set into excellent agreement with the experimental fundamentals; for example, in naphthalene, the average absolute error is 4.4  $\text{cm}^{-1}$  and the maximum error is 12.4  $\text{cm}^{-1}$ . To calibrate the intensities, we have performed B3LYP calculations on naphthalene, and the naphthalene and 1- and 2-hydronaphthalene cations, as well as pyrene, and the pyrene and 1-, 2-, and 4-hydropyrene cations using the 6-31 + G\* and 6-31 + + G\*\* basis sets. The computed ratios of the intensities obtained using these higher level basis sets to those obtained using the 4-31G basis set are presented in Table 1. Excluding the naphthalene cation in the 6-31 + + G\*\* basis set, improving the basis set generally reduces the aromatic C–H stretching intensity. For the pyrene species considered, this reduction is found to be as large as two- to fourfold. While the impact of the higher level basis sets is more ambiguous for the naphthalene species, it should be noted that the absolute intensities of the aromatic CH stretching modes in these species are very small, tending to exaggerate the relative impact of any variations in the calculations. For example, in the naphthalene cation, the aromatic C–H stretch intensity changes from 1.45  $\text{km/mol}$  in the 4-31G basis set

Table 1

The basis set dependence of the calculated total aromatic and aliphatic CH stretching intensities for the naphthalene and pyrene species considered in Section 3.2, compared with that of the remaining, non-CH stretching modes in those species

Species	6-31 + G*/4-31G		6-31 + + G**/4-31G	
	CH stretching modes		All other modes	
	Aromatic	Aliphatic	Aromatic	Aliphatic
$\text{C}_{10}\text{H}_8$	0.87		0.83	
$\text{C}_{10}\text{H}_8^+$	0.83		0.92	
$\text{C}_{10}\text{H}_9^{\text{a}}$	0.68	0.95	0.94	
$\text{C}_{16}\text{H}_{10}$	0.86		0.85	
$\text{C}_{16}\text{H}_{10}^+$	0.56		0.92	
$\text{C}_{16}\text{H}_{11}^{\text{b}}$	0.61	0.93	0.94	
			0.71	1.12
			1.98	0.95
			0.98	1.08
			0.71	1.06
			0.27	0.95
			0.39	1.13
				0.97

<sup>a</sup> Average for two possible hydronaphthalene cation structures.

<sup>b</sup> Average for three possible hydropyrene cation structures.

to 2.86 km/mol for the 6-31 + + G\*\* basis set; so while the ratio is much larger than 1, the absolute change is small. Thus, the calibration data provided by the pyrene system is expected to provide a more realistic assessment of the accuracy of the calculations for PAH species as a whole.

Interestingly, unlike the aromatic C–H stretching intensity, the aliphatic C–H stretching intensities and the total non-C–H stretching intensities are relatively independent of the basis set used. Thus this work, along with previous work [36,43], indicates that, while the 4-31G intensities of non-C–H stretching modes in PAHs are reasonably accurate, the aromatic C–H stretching intensities are too large by some two- to threefold. The current work also shows that, unlike their aromatic counterparts, the accuracy of the computed aliphatic C–H stretching intensities is comparable with that of the non-C–H stretching modes. Thus, the overestimation of the intensities with the 4-31G basis set appears to be limited specifically to the aromatic C–H stretching modes. Therefore, since this effect is variable in magnitude and limited to only a single class of modes, we report the 4-31G intensities as computed for all bands with the stipulation that the aromatic CH stretching intensities probably represent an overestimate of their actual intensities. We should also note that, regardless of their composition, when two modes of the same symmetry are close in energy, their relative intensities are sensitive to the level of theory, but the sum of their intensities is very reliable.

The B3LYP calculations were performed using the GAUSSIAN 98 computer codes [61]. The complete harmonic frequencies and intensities, including those obtained with the higher level basis sets, can be found at <http://ccf.arc.nasa.gov/~cbauschl/closed-shell.data>.

### 3. Results

The results of our theoretical analyses of closed-shell PAH cations are presented next, organized according to class, with the infrared spectra of the  $C_{\text{odd}}$  PAH cations considered first, followed by that of the protonated PAH cations.

#### 3.1. Fully benzenoid PAH cations containing an odd number of carbon atoms ( $C_{\text{odd}}$ PAH cations)

These closed-shell PAH cations are fully benzenoid (i.e. composed only of fused six-membered rings) species whose skeleton is composed of an odd number of carbon atoms. This investigation was motivated by the work of Weilmunster, Keller, and Homann [62], who have analyzed the PAH cation structures that are produced in combustion processes, the processes considered most likely involved in the production of interstellar PAHs [63,64]. Employing time-of-flight mass spectrometry to monitor the formation and growth of PAH cations in flames, Weilmunster et al. found that the PAH cations exhibit their own unique growth chemistry, involving species and structures that differ significantly from those found in the neutral PAH population. Not surprisingly, small PAH cations appear first, early in the combustion region, with sequentially larger species becoming important with increasing depths into the combustion region. What is surprising is the distribution of the structures in the flame PAH cation population. They report that, for cations up to about 50 carbon atoms, structures with an odd number of carbon atoms actually dominate the population. Furthermore, the authors determined that these odd carbon number species were not simply species that incorporated a five-membered ring in their structures but were, instead, fully benzenoid structures. Such structures are illustrated in Fig. 1, which shows the structures of the species considered in this work. As one approaches 50 carbon atoms, the populations of the species with even and odd numbers of carbon atoms converge and, above this size, appear in roughly equal proportions. Considering the energetic conditions in many of the infrared emission zones and the inherent stability of the closed-shell Codd PAH cations, if interstellar PAHs are indeed produced under combustion-like conditions in carbon-rich circumstellar shells, such species may well represent important members of the smaller PAH population in these regions.

The results of the aforementioned combustion experiments can be understood in terms of the

electronic structures of the ions involved. Quite simply,  $C_{\text{even}}$  PAH cations necessarily have an open-shell, radical structure, while the  $C_{\text{odd}}$  PAHs have the chemically more favorable closed-shell structure and are therefore preferred. Presumably, by the time one reaches 50 carbon atoms, stability provided by electron delocalization over the extensive aromatic framework dilutes the energetic cost associated with maintaining the odd electron to the point that there is no longer any significant preference for closed-shell over open-shell structures.

Synthetic representations of the theoretically calculated infrared spectra of several  $C_{\text{odd}}$  PAH cations ranging from  $C_{13}H_9^+$  to  $C_{59}H_{19}^+$  are presented in Fig. 3. These simulations were generated by assigning each calculated band a  $20\text{ cm}^{-1}$  full-width at half-height (FWHH) gaussian profile of the appropriate intensity. Such a profile is consistent with that expected from molecules emitting under the conditions of the interstellar problem [26]. Abbreviated tabulations of the calculated band positions, symmetries, and intensities can be found in Tables 2 and 3. In those tables, the data at frequencies below  $2000\text{ cm}^{-1}$  have been truncated at the 10% level. The infrared active modes in the  $3200\text{--}2800\text{ cm}^{-1}$  CH stretching region are presented in their entirety, in accordance with their more diminutive nature and their role in the following discussion. Complete tabulations of the calculated data (including both IR active and inactive modes) have been posted on the Internet at <http://ccf.arc.nasa.gov/~cbauschl/closed-shell.data>. Inspection of these data reveals that each of the spectra are dominated by three strong features in the  $1600\text{--}1100\text{ cm}^{-1}$  ( $6.25\text{--}9.1\text{ }\mu\text{m}$ ) region, which is characteristic of aromatic CC stretching and CH in-plane wagging vibrations. In some cases, these features represent a single very strong band, while in others they reflect an overlapping of two or more features that fall close to each other (see Tables 2 and 3). The band near  $1600\text{ cm}^{-1}$  (a strong doublet in the spectrum of  $C_{13}H_9^+$ ) is consistently the strongest of these. The other two typically fall in the mid- $1300\text{ cm}^{-1}$  ( $7.5\text{ }\mu\text{m}$ ) and the low  $1200\text{ cm}^{-1}$  ( $8.3\text{ }\mu\text{m}$ ) regions. While it is well established that the strongest infrared bands of PAH cations

tend to fall in the  $1600\text{--}1100\text{ cm}^{-1}$  region, it is unusual to find the band near  $1600\text{ cm}^{-1}$  to be the strongest in the spectrum (see, for example, Figs. 6–9). It is also unusual to see such a similarity in the pattern of these strong bands over such a large range of molecular sizes. Indeed, comparison of the spectra in Fig. 3 with the data currently available in the literature [39–55] shows that, throughout the infrared, the spectral variations of  $C_{\text{odd}}$  PAHs over a wide range of molecular sizes are more subtle than those of neutral PAHs and PAH radical cations. They are also more subtle than those found for the closed-shell protonated PAH cations that are discussed in Section 3.2 (for reference, compare also the spectra of the naphthalene radical cation and the circumcoronene radical cation in Fig. 6a and Fig. 9b, respectively). At this stage, it is unclear whether this is a characteristic of the particular series of molecules studied, or whether this is a general feature of this class of PAH cation. Another interesting aspect of this region of the spectrum is the size dependence of the dominant band positions. Specifically, highest frequency features in this region all tend to cluster between  $1595$  and  $1575\text{ cm}^{-1}$ , and show little dependence on molecular size. The positions of the other two dominant bands, on the other hand, shift steadily toward lower frequencies with increasing molecular size from  $1361$  and  $1259\text{ cm}^{-1}$  ( $7.4$  and  $7.94\text{ }\mu\text{m}$ ) in the  $C_{13}H_9^+$  cation to  $1318$  and  $1189\text{ cm}^{-1}$  ( $7.6$  and  $8.4\text{ }\mu\text{m}$ ) in the  $C_{59}H_{19}^+$  cation. This behavior stands in marked contrast to that of PAH radical cations [56] where it is the bands near  $1600\text{ cm}^{-1}$  that shift to higher frequencies with increasing molecular size, while the bands near  $1300\text{ cm}^{-1}$  remain more or less static. In both cases, however, the net effect is an increase in the spacing between these features.

A final noteworthy aspect of this series of spectra is the molecular size dependence of the aromatic CH stretching features in the  $3100\text{--}3050\text{ cm}^{-1}$  ( $3.23\text{--}3.28\text{ }\mu\text{m}$ ) range. First, inspection of the data in Tables 2 and 3 shows that the position of the dominant CH stretching feature undergoes a distinct red shift with increasing molecular size, decreasing from a maximum of  $3106\text{ cm}^{-1}$  ( $3.22\text{ }\mu\text{m}$ ) in the  $C_{13}H_9^+$  cation down to  $3078\text{ cm}^{-1}$  ( $3.25\text{ }\mu\text{m}$ ) for the  $C_{59}H_{19}^+$  cation. At the same time,

Table 2  
 Calculated frequencies, symmetries, and intensities for the infrared active modes of the  $C_{13}H_9^+$ ,  $C_{19}H_{11}^+$ , and  $C_{27}H_{13}^+$  cations<sup>a</sup>

$C_{13}H_9^+$			$C_{19}H_{11}^+$			$C_{27}H_{13}^+$					
$\tilde{\nu}$ ( $cm^{-1}$ )	Symmetry	Intensity (km/mol)	$I_{rel}$	$\tilde{\nu}$ ( $cm^{-1}$ )	Symmetry	Intensity (km/mol)	$I_{rel}$	$\tilde{\nu}$ ( $cm^{-1}$ )	Symmetry	Intensity (km/mol)	$I_{rel}$
187.4	A <sub>2</sub> '	12.39	0.055	864.4	A''	78.68	0.169	872.6	B <sub>1</sub>	77.80	0.286
750.7	A <sub>2</sub> '	67.08	0.296	1226.4	A'	158.49	0.340	924.2	B <sub>1</sub>	80.37	0.296
855.3	A <sub>2</sub> '	73.70	0.326	1351.1	A'	108.77	0.233	1188.3	A <sub>1</sub>	33.15	0.122
1120.6	E'	49.68	0.219	1364.8	A'	50.86	0.109	1215.2	A <sub>1</sub>	140.85	0.518
1206.7	E'	33.32	0.147	1396.3	A'	120.77	0.259	1216.1	B <sub>2</sub>	103.13	0.380
1259.5	E'	166.04	0.733	1546.6	A'	53.56	0.115	1267.4	A <sub>1</sub>	43.97	0.162
1361.1	E'	170.86	0.755	1566.8	A'	61.16	0.131	1349.6	B <sub>2</sub>	148.44	0.546
1543.6	E'	158.04	0.698	1594.9	A'	466.81	1.00	1354.3	A <sub>1</sub>	221.44	0.815
1581.8	E'	226.42	1.00					1460.3	A <sub>1</sub>	55.64	0.205
								1548.0	B <sub>2</sub>	33.17	0.122
								1571.7	B <sub>2</sub>	154.66	0.569
								1580.5	A <sub>1</sub>	271.72	1.00
								1597.7	A <sub>1</sub>	232.25	0.855
3072.9	E'	0.38	0.002	3061.7	A'	0.54	0.001	3061.5	B <sub>2</sub>	1.90	0.007
3076.8	E'	0.50	0.002	3072.0	A'	0.77	0.002	3061.6	A <sub>1</sub>	0.19	0.001
3105.7	E'	1.72	0.008	3075.5	A'	1.62	0.003	3066.1	B <sub>2</sub>	0.45	0.002
				3087.1	A'	2.22	0.005	3067.2	A <sub>1</sub>	0.66	0.002
				3088.8	A'	9.25	0.020	3068.2	A <sub>1</sub>	0.29	0.001
				3101.3	A'	7.38	0.016	3070.3	A <sub>1</sub>	0.65	0.002
				3101.4	A'	1.25	0.003	3073.3	B <sub>2</sub>	1.96	0.007
								3083.6	A <sub>1</sub>	6.43	0.024
								3085.1	B <sub>2</sub>	30.55	0.112
								3085.6	A <sub>1</sub>	14.04	0.052
								3099.9	A <sub>1</sub>	8.37	0.031

<sup>a</sup> The data for  $\tilde{\nu} < 2000\text{ cm}^{-1}$  have been truncated at the 10% level. The complete data are tabulated at <http://ccf.arc.nasa.gov/~cbauschl/closed-shell.data>.

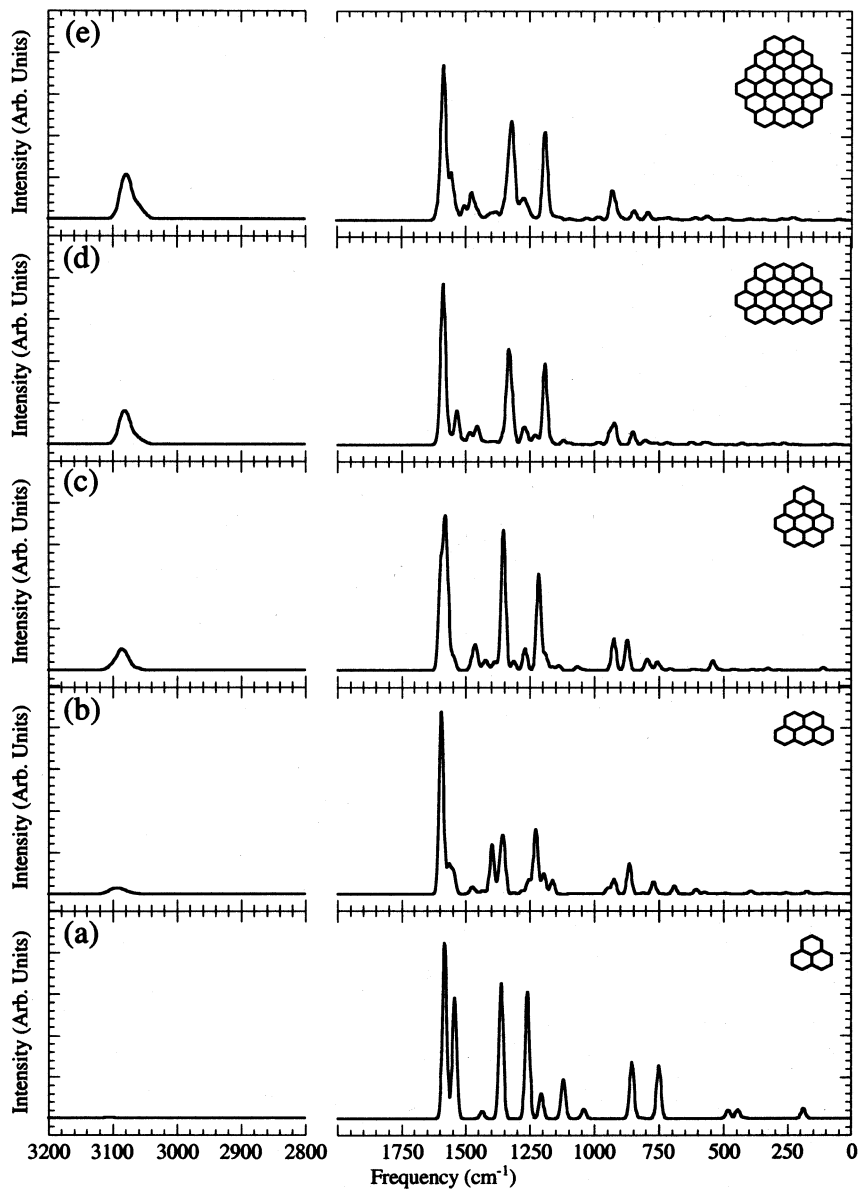


Fig. 3. Representations of the B3LYP computed IR spectra of (a)  $C_{13}H_9^+$ , (b)  $C_{19}H_{11}^+$ , (c)  $C_{27}H_{13}^+$ , (d)  $C_{47}H_{17}^+$ , and (e)  $C_{59}H_{19}^+$ . These simulations were generated by assigning each calculated band a  $20\text{ cm}^{-1}$  FWHH gaussian profile of the appropriate intensity.

the intrinsic intensity per CH group of these modes increases from  $0.30\text{ km/mol}\cdot\text{CH group}$  for  $C_{13}H_9^+$  ( $2.6\text{ km/mol} \div 9\text{ CH groups}$ ) to  $15.3\text{ km/mol}\cdot\text{CH group}$  for  $C_{59}H_{19}^+$  ( $290\text{ km/mol} \div 19\text{ CH groups}$ ). Note that, while the absolute intensities of these modes have not been corrected for the expected computational overestimate, the varia-

tion that is reflected in these numbers should be independent of that correction (the same correction likely applies to all the numbers). Although some increase in the intensity of the CH stretching features is expected simply on the basis of the increasing number of aromatic CH groups in the molecule, the observed magnitude of this effect is

Table 3

Calculated frequencies, symmetries, and intensities for the infrared active modes of the  $C_{47}H_{17}^+$  and  $C_{59}H_{19}^+$  cations<sup>a</sup>

$C_{47}H_{17}^+$				$C_{59}H_{19}^+$			
$\tilde{\nu}$ ( $cm^{-1}$ )	Symmetry	Intensity (km/mol)	$I_{rel}$	$\tilde{\nu}$ ( $cm^{-1}$ )	Symmetry	Intensity (km/mol)	$I_{rel}$
850.4	B <sub>1</sub>	61.64	0.108	792.2	B <sub>1</sub>	35.57	0.100
920.4	B <sub>1</sub>	103.42	0.181	845.3	B <sub>1</sub>	41.92	0.118
938.5	B <sub>1</sub>	64.00	0.112	919.0	B <sub>1</sub>	72.39	0.204
1188.9	B <sub>2</sub>	143.36	0.250	932.7	B <sub>1</sub>	123.00	0.347
1190.8	A <sub>1</sub>	142.30	0.249	1184.5	A <sub>1</sub>	183.27	0.517
1192.1	B <sub>2</sub>	127.24	0.222	1189.9	B <sub>2</sub>	103.56	0.292
1275.0	A <sub>1</sub>	60.17	0.105	1192.8	B <sub>2</sub>	91.41	0.258
1317.5	B <sub>2</sub>	178.04	0.311	1193.7	A <sub>1</sub>	116.40	0.328
1331.7	A <sub>1</sub>	173.37	0.303	1254.2	A <sub>1</sub>	46.58	0.131
1331.9	B <sub>2</sub>	259.21	0.453	1270.1	A <sub>1</sub>	83.02	0.234
1483.1	A <sub>1</sub>	59.42	0.104	1286.3	A <sub>1</sub>	50.94	0.144
1532.7	B <sub>2</sub>	172.33	0.301	1306.4	A <sub>1</sub>	73.64	0.208
1580.1	A <sub>1</sub>	235.10	0.411	1314.1	B <sub>2</sub>	297.25	0.838
1583.4	B <sub>2</sub>	102.08	0.178	1323.5	A <sub>1</sub>	199.73	0.563
1589.3	B <sub>2</sub>	572.48	1.00	1331.0	A <sub>1</sub>	121.28	0.342
				1340.0	B <sub>2</sub>	52.95	0.149
				1351.0	A <sub>1</sub>	40.38	0.114
				1474.9	B <sub>2</sub>	72.74	0.205
				1477.1	A <sub>1</sub>	43.08	0.121
				1503.6	B <sub>2</sub>	64.38	0.181
				1553.9	A <sub>1</sub>	211.63	0.597
				1575.4	A <sub>1</sub>	113.48	0.320
				1581.3	B <sub>2</sub>	306.42	0.864
				1585.1	A <sub>1</sub>	354.75	1.00
				1592.6	A <sub>1</sub>	90.04	0.254
				1604.2	B <sub>2</sub>	47.38	0.134
3057.3	A <sub>1</sub>	2.19	0.004	3055.3	A <sub>1</sub>	0.98	0.003
3057.3	B <sub>2</sub>	5.73	0.010	3055.8	A <sub>1</sub>	3.02	0.009
3059.7	A <sub>1</sub>	6.84	0.012	3057.1	B <sub>2</sub>	3.43	0.010
3060.1	A <sub>1</sub>	5.34	0.009	3057.3	A <sub>1</sub>	11.06	0.031
3061.6	B <sub>2</sub>	0.98	0.002	3058.2	B <sub>2</sub>	17.34	0.049
3062.6	A <sub>1</sub>	6.67	0.012	3058.4	A <sub>1</sub>	0.23	0.001
3063.0	B <sub>2</sub>	1.83	0.003	3059.5	B <sub>2</sub>	11.98	0.034
3063.1	A <sub>1</sub>	0.93	0.002	3060.0	A <sub>1</sub>	4.71	0.013
3079.5	B <sub>2</sub>	6.90	0.012	3060.7	B <sub>2</sub>	1.38	0.004
3079.8	A <sub>1</sub>	20.76	0.036	3060.8	A <sub>1</sub>	1.37	0.004
3080.0	B <sub>2</sub>	19.77	0.035	3062.9	B <sub>2</sub>	3.49	0.010
3080.1	A <sub>1</sub>	34.34	0.060	3077.3	B <sub>2</sub>	6.04	0.017
3082.1	B <sub>2</sub>	71.29	0.125	3077.6	A <sub>1</sub>	45.76	0.129
3082.3	A <sub>1</sub>	19	0.033	3078.1	B <sub>2</sub>	90.84	0.256
				3078.2	A <sub>1</sub>	21.84	0.062
				3080.2	B <sub>2</sub>	7.34	0.021
				3082.0	A <sub>1</sub>	59.18	0.167

<sup>a</sup> The data for  $\tilde{\nu} < 2000$   $cm^{-1}$  have been truncated at the 10% level. The complete data are tabulated at <http://ccf.arc.nasa.gov/~cbauschl/closed-shell.data>.

greater than can be explained by this factor alone. This trend is understandable in terms of the variations in the charge distribution within the cations, and the localized nature of the CH stretching modes. In general, extensive electron delocalization within these species leads to an effective distribution of the positive charge throughout the molecule. Consequently, the charge density across the cation decreases in proportion to the area of the PAH structure. The CH bonds (and their associated stretching modes), on the other hand, are confined to the periphery of the structure and, therefore, increase in number only in proportion to the circumference of the molecule. Thus, as the size of the cation increases, the increase in the number of CH groups cannot completely compensate for the reduced charge density and there is a steady decrease in the net oscillating charge associated with the CH stretching vibrations. This implies that the character of the CH stretching vibrations in the cation should approach that of the neutral species with increasing molecular size. This is exactly what is reflected in the spectrum in the form of a substantial relaxation of the dramatic suppression that these modes experience upon ionization [27,35,36,39–55].

It should be noted that this effect is not expected to appreciably impact the other classes of vibrations within the molecule. The CC stretching modes, for example, typically involve the entire carbon skeleton of the molecule. Thus, the region associated with these modes scales as the area of the molecule, neutralizing the effect of the charge dilution. Furthermore, despite the fact that the CH in-plane bends, in principle, depend on the number of CH groups, these modes mix much more effectively with the CC stretches and, again, the effect of charge dilution is largely nullified. Finally, the intensities of the CH out-of-plane modes are similar between the cation and the neutral species and, consequently, little variation would be expected to accompany a transition from cation to quasi-neutral character in the CH groups.

### 3.2. Protonated PAH Cations (HPAH<sup>+</sup>)

In recent selected-ion flow tube experiments, Le Page et al. [23] and Snow et al. [24] explored the

reactivity of ionized PAH structures with various simple atomic and molecular species of interstellar relevance. Of particular interest, they found that the radical cations of benzene, naphthalene, and pyrene reacted readily with atomic hydrogen, but were relatively unreactive toward molecular hydrogen. Furthermore, the HPAH<sup>+</sup> species thus formed were found to be relatively unreactive toward additional H atoms. Note that, while reaction with a hydrogen atom is not strictly a protonation reaction (i.e. the addition of H<sup>+</sup>), the product in this case (HPAH<sup>+</sup>) is identical to that obtained from the addition of a proton to a neutral PAH molecule, and thus is referred to here as a 'protonated' PAH. These results are consistent with the studies of Weilmunster et al. described in Section 3.1, which also bear on this issue. In those studies, in contrast to the C<sub>odd</sub> PAH cations, the PAH cations containing an even number of carbon atoms were found to exist predominantly in the protonated form. Together, these experiments indicate that PAH radical cations readily add an H atom while closed-shell ion structures do not.

These results are again understandable in terms of the electronic structures of the ions involved. The radical cations, with their highly reactive, open-shell structures, readily add a hydrogen atom (also having a single, unpaired electron) to produce a cation with a more favorable closed-shell electron configuration. The resultant protonated cation is far less reactive with H atoms because it already has the preferred closed-shell electronic structure and addition of another H atom would thus disrupt this favorable configuration. The theoretical calculations carried out here are consistent with this interpretation. For example, consider the sequential addition of H atoms to the naphthalene radical cation (C<sub>10</sub>H<sub>8</sub><sup>+</sup>). While calculations at the B3LYP/4-31G level reveal no barrier to the addition of an H atom to the naphthalene radical cation, they do qualitatively indicate the presence of a barrier to the addition of a second hydrogen atom (forming C<sub>10</sub>H<sub>9</sub><sup>+</sup> and C<sub>10</sub>H<sub>10</sub><sup>+</sup>, respectively). The experimental results indicate that this barrier must be of sufficient magnitude to measurably affect the reactivity of these species even at large thermal energies (i.e. in a flame). The calculations further indicate that, while there is no barrier to the addition of a

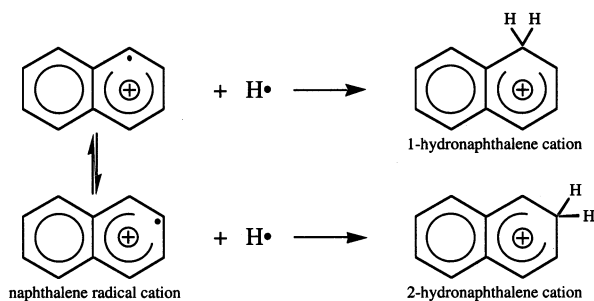


Fig. 4. An illustration of the reaction of the naphthalene radical cation ( $C_{10}H_8^{\bullet+}$ ) with atomic hydrogen showing the two possible structural isomers of the hydronaphthalene cation product.

third H atom, there is once again a barrier to the addition of a fourth (forming  $C_{10}H_{11}^+$  and  $C_{10}H_{12}^+$ , respectively). Again, this is presumably a reflection of the inherently greater reactivity of the open-shell electronic structure. Thus, in general, once formed, the closed-shell, protonated PAH structure represents a bottleneck in the further hydrogenation of interstellar PAH cations, moderating the degree of hydrogenation achieved by the interstellar PAH population and favoring those  $H_nPAH^+$  species in which  $n$  is odd. Nevertheless, given the great interstellar abundance of hydrogen, the formation of hydrogenated PAH cations with some modest loss of aromatic character is expected to be a natural consequence of the presence of PAH ions in the ISM.

Consider again the reaction between the naph-

thalene radical cation,  $C_{10}H_8^{\bullet+}$ , and an H atom. This reaction and the topology of its associated potential energy surface are illustrated in Figs. 4 and 5, respectively. The calculations indicate that the  $C_{10}H_8^{\bullet+} + H$  reaction is exothermic by 259 kJ/mol. Thus, in the absence of a reaction barrier, the rapid reaction observed in the laboratory is understandable [23,24,62]. As already discussed, the primary driving force for this reaction lies in the pairing of the parent radical cation's odd electron. It should be emphasized that these and the other protonated PAH cations discussed later do not arise merely from an electrostatic attraction between the H atom and the PAH cation, but are, in fact, fully covalently bound ions. Consequently, the addition reaction results in the formation of an aliphatic  $sp^3$ -hybridized carbon atom that no longer participates in the delocalized  $\pi$  molecular orbital of the aromatic carbon skeleton, reducing the aromaticity of the parent PAH. Inspection of Fig. 4 reveals that, for naphthalene, there are two chemically distinct products of H atom addition: 1- and 2-hydronaphthalene cation, with the former more stable by 13.4 kJ/mol. The calculations indicate that there is no significant barrier to H-atom addition at either of the two possible sites, and that the barrier to isomerization between the two structures ( $\approx 71$  kJ/mol) is small compared with the energy liberated in the H addition reaction (see Fig. 5). Together, these results imply that the two isomers would probably be formed in roughly the statistical ratio (1:1)

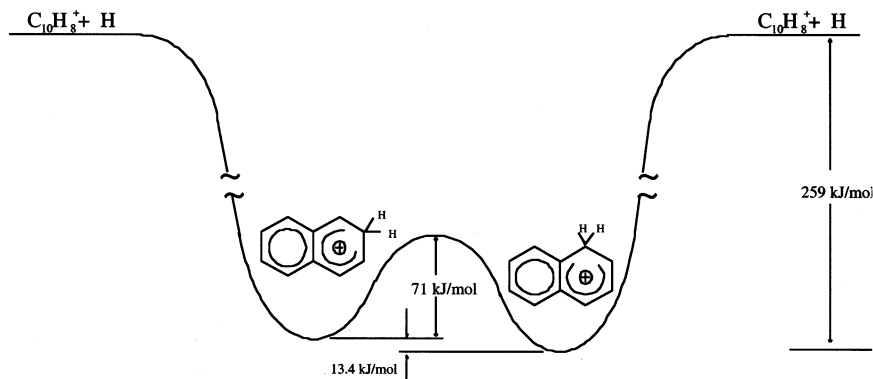


Fig. 5. A potential energy diagram for the  $C_{10}H_8^{\bullet+} + H^{\bullet}$  reaction. All numerical values were obtained using DFT at the B3LYP/4-31G level.

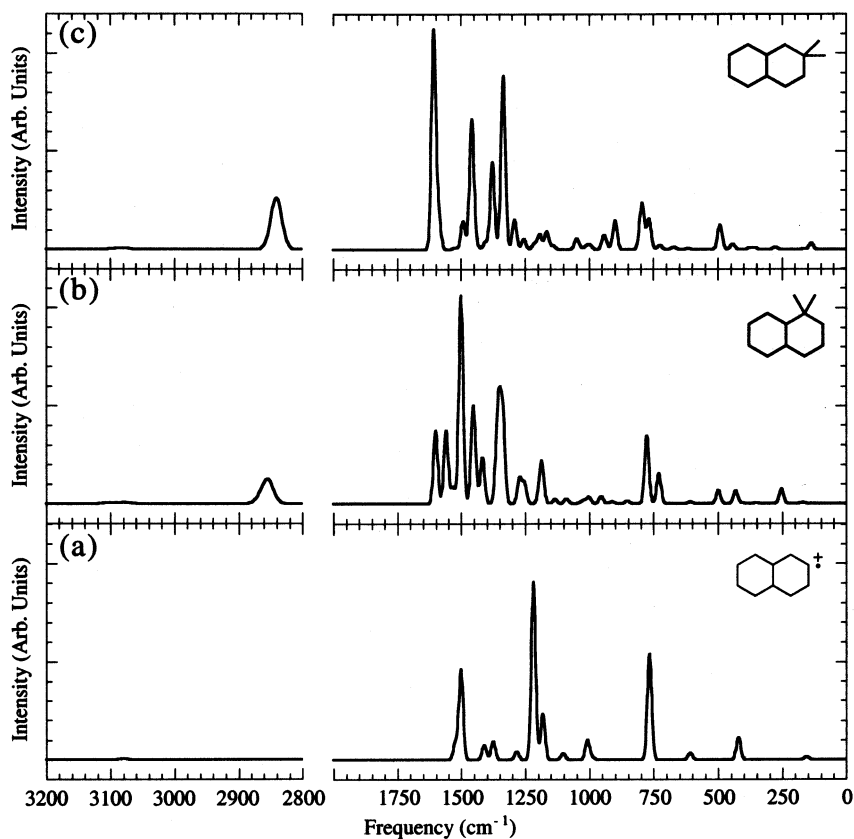


Fig. 6. The B3LYP computed IR spectra of the (b) 1-hydronaphthalene and (c) 2-hydronaphthalene cations (both C<sub>10</sub>H<sub>9</sub><sup>+</sup>) compared with that of the naphthalene radical cation, C<sub>10</sub>H<sub>8</sub><sup>+</sup> (a). Full-width at half-maximum (FWHM), 20 cm<sup>-1</sup>.

under interstellar conditions. The sequential addition of a second hydrogen atom to form the 1,2-dihydronaphthalene cation is exothermic by another 178 kJ/mol but, as already discussed, faces a significant reaction barrier and proceeds at a rate some two orders of magnitude less at room temperature [23,24].

Analogous calculations have been performed for the pyrene, coronene, and circumcoronene radical cations (C<sub>16</sub>H<sub>10</sub><sup>+</sup>, C<sub>24</sub>H<sub>12</sub><sup>+</sup>, and C<sub>54</sub>H<sub>18</sub><sup>+</sup>, respectively), with similar results. As was the case for the naphthalene radical cation, hydrogen atom addition to these cations is exothermic by 251, 229, and 234 kJ/mol, respectively. Examples of the types of structures found in the resulting protonated PAH species are presented in Fig. 2. The pyrene cation has three non-equivalent sites for H atom addition, yielding three unique prod-

ucts: 1-hydropyrene, 2-hydropyrene, and 4-hydropyrene (C<sub>16</sub>H<sub>11</sub><sup>+</sup>). The most stable product is the 1-hydropyrene, with the 2- and 4-hydropyrenes lying 63.2 and 45.2 kJ/mol higher in energy, respectively. For the coronene cation, all the positions for H atom addition are equivalent, yielding only one chemically unique protonated cation structure (C<sub>24</sub>H<sub>13</sub><sup>+</sup>). For the circumcoronene cation, there are again two possible non-equivalent products, 1- and 3-hydrocircumcoronene (C<sub>54</sub>H<sub>19</sub><sup>+</sup>). In this case, the 3-hydrocircumcoronene is calculated to be the lower energy structure, with the 1-hydrocircumcoronene lying 52.3 kJ/mol higher in energy.

Representations of the calculated infrared spectra of the 1- and 2-hydronaphthalene cations are shown in Fig. 6, and the salient band positions and intensities are tabulated in Table 4. For refer-

ence, the spectrum of the naphthalene cation is also shown in the figure. The spectra of the 1-, 2-, and 4-hydropyrene cations are shown together with that of the parent pyrene cation in Fig. 7. The prominent band positions and intensities for the protonated species are presented in Table 5. The spectrum of the 1-hydrocoronene cation is shown referenced to that of the parent coronene cation in Fig. 8, and tabulated in Table 6. The spectra of the 1- and 3-hydrocircumcoronene cations are shown in Fig. 9 and the positions of the prominent bands in these spectra are reported in Table 7. The spectra of neutral circumcoronene and the circumcoronene radical cation have not been reported previously and are also included in Fig. 9. The salient bands of these species are summarized Table 8. In all cases, spectral simulations were generated by assigning each calculated band a 20  $\text{cm}^{-1}$  FWHH gaussian profile of the appropriate intensity. In addition, in accordance with space limitations, the data for  $\tilde{\nu} < 2000 \text{ cm}^{-1}$

have been truncated at the 10% level in the tables. However, the infrared active modes in the 3200–2800  $\text{cm}^{-1}$  region are reported in their entirety. Complete tabulations of the calculated data (including both IR active and inactive modes) have been posted on the Internet at <http://ccf.arc.nasa.gov/~cbauschl/closed-shell.data>.

Again, as has been the case for PAH radical cations and the  $C_{\text{odd}}$  cations already presented, these spectra are all dominated by the aromatic CC stretching and CH in-plane wagging modes in the 1600–1200  $\text{cm}^{-1}$  region. Inspection of Figs. 6–9 shows that, in general, the spectra of the protonated PAHs considered here are substantially more complicated than those of the  $C_{\text{odd}}$  cations discussed in Section 3.1. Indeed, comparison of the spectra of the protonated species with that of their parent radical cation indicates that H atom addition is accompanied by a marked increase in spectral complexity through this region. This is not surprising since H atom addition

Table 4

Calculated frequencies, symmetries, and intensities for the infrared active modes of the 1-hydronaphthalene and 2-hydronaphthalene cations,  $C_{10}H_9^+$ <sup>a</sup>

1-Hydronaphthalene				2-Hydronaphthalene			
$\tilde{\nu}$ ( $\text{cm}^{-1}$ )	Symmetry	Intensity (km/mol)	$I_{\text{rel}}$	$\tilde{\nu}$ ( $\text{cm}^{-1}$ )	Symmetry	Intensity (km/mol)	$I_{\text{rel}}$
729.9	A''	28.71	0.128	766.8	A''	30.09	0.127
776.3	A''	73.53	0.327	794.1	A''	46.94	0.198
1187.1	A'	26.61	0.118	1290.8	A'	32.43	0.136
1271.5	A'	28.03	0.125	1334.2	A'	179.50	0.755
1336.2	A'	91.12	0.406	1377.5	A'	94.48	0.398
1351.2	A'	89.74	0.399	1457.8	A'	141.20	0.594
1361.8	A'	34.68	0.154	1491.9	A'	31.05	0.131
1416.4	A'	50.41	0.224	1586.9	A'	36.02	0.152
1453.0	A'	106.28	0.473	1606.9	A'	237.63	1.00
1500.1	A'	224.69	1.00				
1558.9	A'	80.12	0.357				
1599.9	A'	79.08	0.352				
2854.2	A'	24.01	0.107	2839.5	A'	46.62	0.196
2865.7	A''	6.36	0.028	2844.0	A''	10.13	0.043
3075.0	A'	0.39	0.002	3062.7	A'	0.33	0.001
3079.0	A'	1.00	0.004	3079.0	A'	1.39	0.006
3080.1	A'	0.15	0.001	3093.8	A'	0.33	0.001
3091.3	A'	0.65	0.003	3097.1	A'	0.52	0.002
3107.3	A'	0.76	0.003	3107.8	A'	0.19	0.001

<sup>a</sup> The data for  $\tilde{\nu} < 2000 \text{ cm}^{-1}$  have been truncated at the 10% level. The complete data are tabulated at <http://ccf.arc.nasa.gov/~cbauschl/closed-shell.data>.

Table 5  
 Calculated frequencies, symmetries, and intensities for the infrared active modes of the 1-hydrypyrene, 2-hydrypyrene, and 4-hydrypyrene cations, C<sub>16</sub>H<sub>11</sub><sup>+</sup><sup>a</sup>

1-Hydrypyrene				2-Hydrypyrene				4-Hydrypyrene			
$\tilde{\nu}$ (cm <sup>-1</sup> )	Symmetry	Intensity (km/mol)	<i>I</i> <sub>rel</sub>	$\tilde{\nu}$ (cm <sup>-1</sup> )	Symmetry	Intensity (km/mol)	<i>I</i> <sub>rel</sub>	$\tilde{\nu}$ (cm <sup>-1</sup> )	Symmetry	Intensity (km/mol)	<i>I</i> <sub>rel</sub>
869.4	A''	103.33	0.398	737.7	B <sub>1</sub>	39.11	0.247	702.3	A''	35.49	0.218
1208.1	A'	40.95	0.158	850.6	B <sub>1</sub>	97.81	0.617	848.0	A''	102.56	0.631
1230.7	A'	139.91	0.539	936.8	A <sub>1</sub>	15.97	0.101	1206.3	A'	21.01	0.129
1241.1	A'	45.68	0.176	953.2	B <sub>1</sub>	27.81	0.176	1237.5	A'	24.56	0.151
1352.6	A'	38.58	0.149	998.5	A <sub>1</sub>	20.34	0.128	1242.9	A'	21.63	0.133
1356.9	A'	48.09	0.185	1074.7	B <sub>2</sub>	20.36	0.128	1314.9	A'	60.08	0.370
1371.6	A'	99.28	0.382	1189.4	B <sub>2</sub>	24.36	0.154	1358.2	A'	38.28	0.236
1381.9	A'	94.37	0.363	1328.8	A <sub>1</sub>	158.42	1.00	1359.4	A'	81.09	0.499
1476.2	A'	58.87	0.227	1331.4	B <sub>2</sub>	76.09	0.480	1372.1	A'	143.39	0.882
1522.2	A'	144.99	0.558	1347.0	B <sub>2</sub>	47.50	0.300	1412.3	A'	60.49	0.372
1554.0	A'	98.76	0.380	1399.3	A <sub>1</sub>	25.36	0.160	1437.0	A'	27.68	0.170
1562.8	A'	127.23	0.490	1414.0	A <sub>1</sub>	88.59	0.559	1466.3	A'	55.06	0.339
1587.1	A'	259.64	1.00	1462.2	B <sub>2</sub>	81.48	0.514	1499.1	A'	41.37	0.255
1613.7	A'	45.94	0.177	1498.2	B <sub>2</sub>	35.10	0.222	1541.6	A'	33.69	0.207
				1546.8	A <sub>1</sub>	119.56	0.755	1575.8	A'	61.51	0.379
				1589.3	B <sub>2</sub>	51.53	0.325	1584.6	A'	48.54	0.299
				1603.9	A <sub>1</sub>	75.33	0.475	1607.5	A'	162.51	1.00
2865.1	A'	16.62	0.064	2843.6	A <sub>1</sub>	39.12	0.247	2848.1	A'	26.81	0.165
2879.3	A''	0.60	0.002	2848.9	B <sub>1</sub>	7.69	0.049	2858.3	A''	2.80	0.017
3073.0	A'	0.33	0.001	3074.7	B <sub>2</sub>	0.16	0.001	3066.8	A'	2.52	0.016
3074.5	A'	0.54	0.002	3075.9	A <sub>1</sub>	0.59	0.004	3071.7	A'	0.23	0.001
3077.4	A'	0.77	0.003	3076.4	A <sub>1</sub>	0.81	0.005	3073.6	A'	0.26	0.002
3085.2	A'	3.22	0.012	3082.6	B <sub>2</sub>	1.92	0.012	3078.1	A'	1.75	0.011
3089.3	A'	1.39	0.005	3090.2	B <sub>2</sub>	9.34	0.059	3089.9	A'	5.45	0.034
3091.6	A'	5.96	0.023	3097.2	A <sub>1</sub>	5.55	0.035	3096.1	A'	6.76	0.042
3102.7	A'	3.47	0.013					3105.6	A'	1.04	0.006

<sup>a</sup> The data for  $\tilde{\nu} < 2000$  cm<sup>-1</sup> have been truncated at the 10% level. The complete data are tabulated at <<http://ccf.arc.nasa.gov/~cbauschi/closed-shell.data>>.

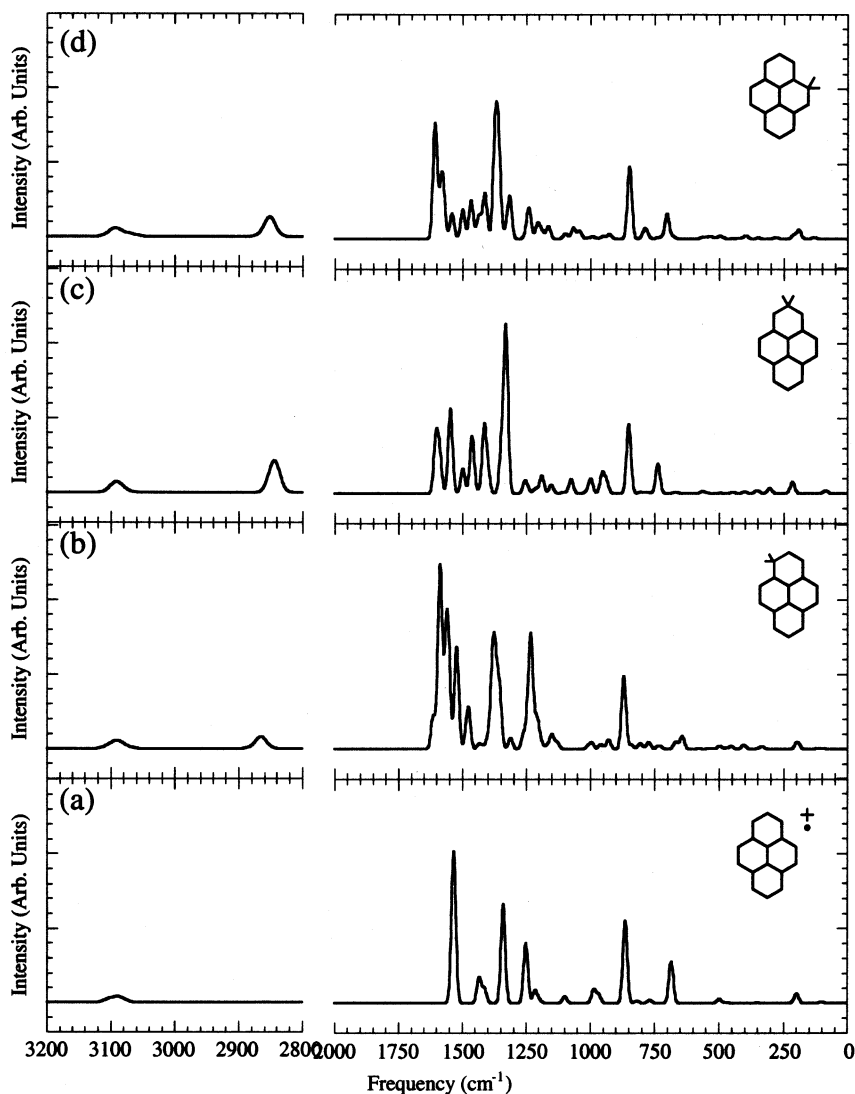


Fig. 7. The B3LYP computed IR spectra of the pyrene radical cation,  $C_{16}H_{10}^{\bullet+}$  (a), is shown together with the spectra of (b) the 1-hydropyrene cation, (c) the 2-hydropyrene cation, and (d) the 4-hydropyrene cation (all  $C_{16}H_{11}^+$ ). FWHM,  $20\text{ cm}^{-1}$ .

reduces the molecular symmetry, thereby increasing the number of infrared active modes and/or enhancing the IR activity of previously weak modes in the region. In addition, the characteristic deformation modes of the aliphatic  $-\text{CH}_2-$  group in the protonated species also contribute in this region, although these modes mix effectively with the aromatic modes such that there is not a clear distinction between ‘aromatic’ and ‘aliphatic’ modes. This increase in spectral complexity is also

accompanied by an appreciable redistribution of the total intensity amongst the modes in this region. For example, while the total intensities of both the 1-hydro- and 3-hydrocircumcoronene cations (both  $\approx 3500\text{ km/mol}$ ) are similar to that of the parent circumcoronene radical cation ( $\approx 3700\text{ km/mol}$ ), the intensity of the strongest individual band in the spectrum of the 1- and 3-hydrocircumcoronene cations ( $1576.0\text{ cm}^{-1}/196.5\text{ km/mol}$  and  $1577.9\text{ cm}^{-1}/327.6\text{ km/mol}$ ,

respectively; Table 7) are three- to fivefold weaker than the strongest band in the spectrum of the circumcoronene radical cation ( $1571.2\text{ cm}^{-1}/958.1\text{ km/mol}$ ; Table 8). Clearly, a significant fraction of the intensity that is concentrated in the  $1571.2\text{ cm}^{-1}$  mode of the circumcoronene radical cation has been redistributed over the manifold of new infrared active modes in the hydrocircumcoronene cations. Similar behavior is also found between the 1-hydrocoronene cation and the coronene radical cation.

For those species that have more than one chemically unique site, the spectral structure in the  $1600\text{--}1200\text{ cm}^{-1}$  region is quite sensitive to the position of the added H atom. This effect is greatest for the smaller hydronaphthalene and hydropyrene cations, where the added H atom has a relatively greater impact of on the vibrational modes. Nevertheless, the differences between the spectra of the two hydrocircumcoronene cations are not inconsequential. Furthermore, it should be emphasized that this effect is not simply due to differences in the symmetry of the species in question. For example, the 1- and 2-hydronaphthalene cations share the same  $C_s$  symmetry, yet their

spectra (Fig. 6b,c) are widely disparate through the  $1600\text{--}1200\text{ cm}^{-1}$  region. The same is also true for the 1- and 4-hydropyrene cations whose spectra are shown in Fig. 7b,d.

Another aspect of the infrared spectra of protonated PAHs that warrants discussion is the CH stretching region between  $3200$  and  $2800\text{ cm}^{-1}$ . Comparison of this region of the spectra in Figs. 6–9 shows that there is a marked increase in the relative strength in the aromatic CH stretching feature near  $3100\text{ cm}^{-1}$  ( $3.23\text{ }\mu\text{m}$ ) compared with the aliphatic CH stretching feature near  $2850\text{ cm}^{-1}$  ( $3.51\text{ }\mu\text{m}$ ) with increasing molecular size. In the spectra of the 1- and 2-hydronaphthalene cations, the CH stretching region is dominated by the aliphatic feature of the single  $-\text{CH}_2-$  group near  $2850\text{ cm}^{-1}$  ( $3.5\text{ }\mu\text{m}$ ), while the aromatic CH stretching feature near  $3050\text{ cm}^{-1}$  ( $3.28\text{ }\mu\text{m}$ ) is so weak as to be all but invisible. However, the relative intensity of the aromatic feature increases relative to the aliphatic feature in the hydropyrenes and actually dominates the aliphatic feature in the spectra of the hydrocoronene and hydrocircumcoronene cations. Indeed, such a trend is expected simply on the basis of the steady increase

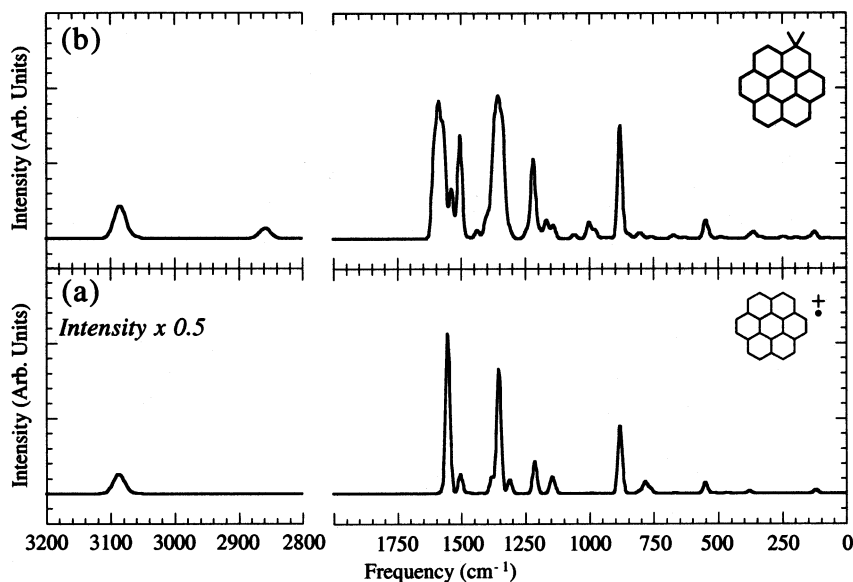


Fig. 8. The B3LYP computed IR spectra of the 1-hydrocoronene cation,  $C_{24}H_{14}^+$  (b), is shown compared with that of the coronene radical cation,  $C_{24}H_{13}^+$  (a). FWHM,  $20\text{ cm}^{-1}$ . The coronene radical cation spectrum has been scaled by 0.5 to facilitate its presentation on the same scale as the hydrocoronene cation.

Table 6

Calculated frequencies, symmetries, and intensities for the infrared active modes of the 1-hydrocoronene cation,  $C_{24}H_{13}^+$ <sup>a</sup>

1-Hydrocoronene			
$\tilde{\nu}$ ( $cm^{-1}$ )	Symmetry	Intensity (km/mol)	$I_{rel}$
548.3	A''	24.68	0.155
880.1	A''	159.27	1.00
1001.0	A'	22.58	0.142
1209.5	A'	21.12	0.133
1218.3	A'	70.47	0.442
1220.9	A'	29.58	0.186
1335.7	A'	137.44	0.863
1349.5	A'	67.75	0.425
1356.1	A'	112.10	0.704
1367.7	A'	48.63	0.305
1372.7	A'	89.28	0.561
1388.4	A'	21.50	0.135
1404.4	A'	18.73	0.118
1503.8	A'	139.25	0.874
1538.4	A'	69.41	0.436
1566.8	A'	130.45	0.819
1579.9	A'	62.32	0.391
1589.2	A'	129.54	0.813
1596.3	A'	18.19	0.114
1606.6	A'	107.72	0.676
2857.5	A'	13.93	0.087
2869.9	A''	0.77	0.005
3062.7	A'	0.20	0.001
3063.5	A'	1.66	0.010
3066.7	A'	0.30	0.002
3067.7	A'	0.36	0.002
3068.8	A'	0.56	0.004
3079.9	A'	6.92	0.043
3083.8	A'	2.15	0.014
3084.8	A'	10.16	0.064
3085.8	A'	19.18	0.120
3088.4	A'	10.02	0.063

<sup>a</sup> The data for  $\tilde{\nu} < 2000$   $cm^{-1}$  have been truncated at the 10% level. The complete data are tabulated at <http://ccf.arc.nasa.gov/~cbauschl/closed-shell.data>.

in the ratio of aromatic CH groups to aliphatic CH groups (hydronaphthalene, 7/2; hydropyrene, 9/2; hydrocoronene, 11/2; hydrocircumcoronene, 17/2; see Fig. 2). However, the data in Tables 4–7 shows that the magnitude of the observed spectral change far exceeds that expected simply on the basis of the increase in the relative number of

aromatic CH groups. In going from hydronaphthalene to hydrocircumcoronene, the ratio of the number of aromatic CH groups to the number of aliphatic CH groups increases by a factor of 2.4 (from 3.5 to 8.5). Over this same range, the calculated ratio of the total aromatic CH stretching intensity ( $\Sigma(3110\text{--}3040$   $cm^{-1}$ ) to the aliphatic CH stretching intensity ( $\Sigma(2900\text{--}2840$   $cm^{-1}$ ) increases from an average of 0.07 for the hydronaphthalenes to 110 for the hydrocircumcoronenes, an increase of nearly 1600-fold. This dramatic shift arises through a combination of two concurrent effects: (1) a reduction in the total intrinsic aliphatic CH stretching intensity by a factor of about 20 (hydronaphthalenes,  $A_{aliphatic} \approx 44$  km/mol; hydrocircumcoronenes,  $A_{aliphatic} \approx 2.3$  km/mol); coupled with (2) an increase in the total intrinsic aromatic CH stretching intensity by a factor of nearly 100 (hydronaphthalenes,  $A_{aromatic} \approx 3$  km/mol; hydrocircumcoronenes,  $A_{aromatic} \approx 250$  km/mol). The enhancement in the intensity of the aromatic CH stretching feature is very similar to that observed in the  $C_{odd}$  PAH cations discussed in Section 3.1, and presumably shares the same origin. The suppression of the aliphatic CH stretching intensity is, on the other hand, more unexpected and not clearly understood at this point.

Finally, it should be noted that the spectrum of neutral circumcoronene has also been calculated as part of this work and is presented along with the cation spectra in Fig. 9. The spectrum of neutral circumcoronene has not been published previously, and it is included here for both its intrinsic merit and as a benchmark for comparison with the various related cationic species. As is typical of neutral PAHs, the spectrum is dominated by the strong aromatic CH stretching feature near 3060  $cm^{-1}$  and the aromatic CH out-of-plane bending mode near 900  $cm^{-1}$ . Both of these features are substantially more intense than any of the CC stretching and CH in-plane bending modes in the 1600–1100  $cm^{-1}$  region. Thus, the significantly increased C/H ratio of the larger PAH molecule (circumcoronene, C/H = 3; coronene, C/H = 2; naphthalene, C/H = 1.25) is

not, in and of itself, sufficient to bring the ratios between the bands in these two regions into agreement with their typical interstellar values. This is consistent with the conclusion that the pattern of band intensities observed in the interstellar spectrum is indicative of a dominant contribution from 'ionized' PAHs.

#### 4. Astrophysical implications

Based on the data already presented, the presence of closed-shell PAH cations in the interstellar infrared emission zones will impact the spectrum in several ways. These are now considered according to spectral region.

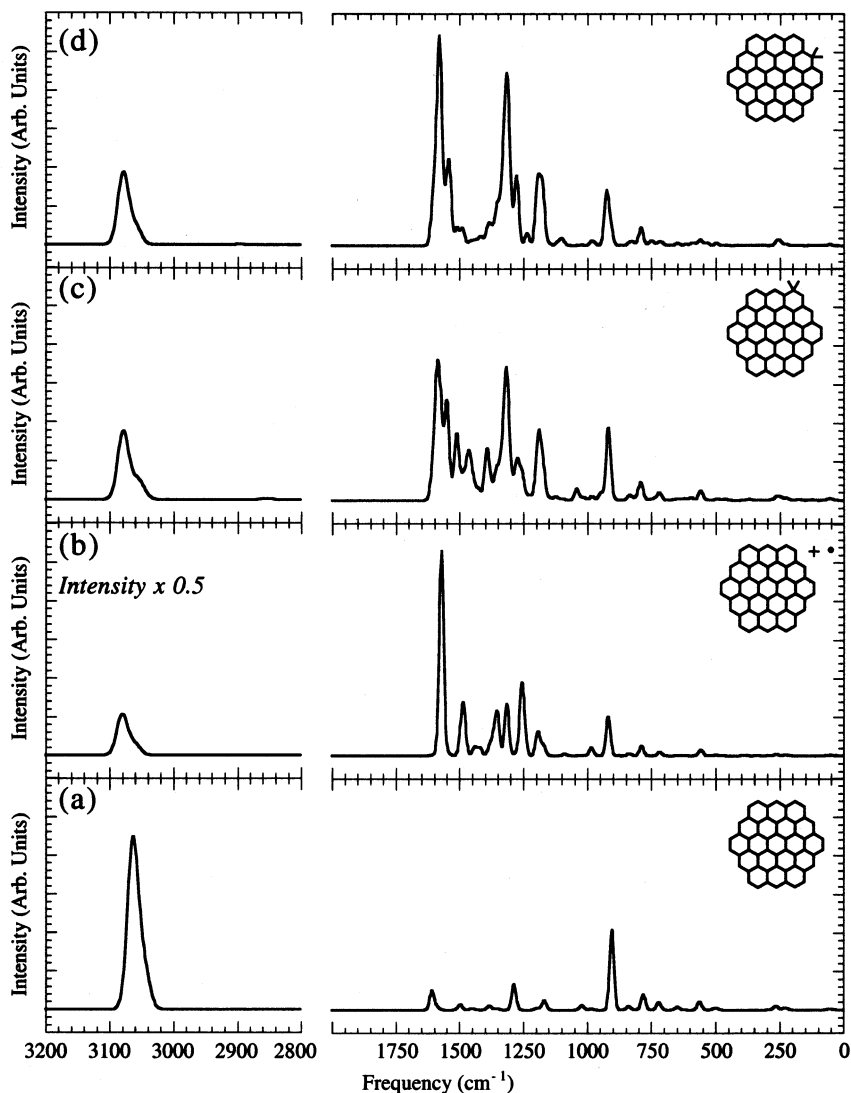


Fig. 9. The B3LYP computed IR spectra of (a) neutral circumcoronene ( $C_{54}H_{18}$ ) and (b) the circumcoronene radical cation ( $C_{54}H_{18}^{+\bullet}$ ), are compared with those of (c) the 1-hydrocircumcoronene and (d) the 3-hydrocircumcoronene cations ( $C_{54}H_{19}^{+}$ ). FWHM,  $20\text{ cm}^{-1}$ . The circumcoronene radical cation spectrum has been scaled by 0.5 to facilitate its presentation on the same scale as the hydrocircumcoronene cations.

Table 7

Calculated frequencies, symmetries, and intensities for the infrared active modes of the 1-hydrocircumcoronene and 3-hydrocircumcoronene cations,  $C_{54}H_{19}^+$  <sup>a</sup>

1-Hydrocircumcoronene				3-Hydrocircumcoronene			
$\tilde{\nu}$ ( $cm^{-1}$ )	Symmetry	Intensity (km/mol)	$I_{rel}$	$\tilde{\nu}$ ( $cm^{-1}$ )	Symmetry	Intensity (km/mol)	$I_{rel}$
790.5	A''	35.91	0.161	791.5	B <sub>1</sub>	48.31	0.129
919.1	A''	189.00	0.846	921.5	B <sub>1</sub>	72.02	0.192
1041.9	A'	31.25	0.140	928.1	B <sub>1</sub>	86.62	0.231
1170.3	A'	23.05	0.103	1176.8	B <sub>2</sub>	124.53	0.332
1173.7	A'	56.61	0.253	1192.9	A <sub>1</sub>	110.37	0.294
1184.1	A'	70.24	0.314	1196.0	B <sub>2</sub>	48.18	0.129
1192.5	A'	126.98	0.568	1273.5	A <sub>1</sub>	40.81	0.109
1250.0	A'	23.68	0.106	1276.4	A <sub>1</sub>	82.98	0.221
1257.7	A'	55.63	0.249	1280.2	A <sub>1</sub>	58.54	0.156
1273.7	A'	68.92	0.308	1303.4	B <sub>2</sub>	126.19	0.337
1290.7	A'	29.75	0.133	1315.0	B <sub>2</sub>	374.85	1.00
1305.1	A'	28.12	0.126	1329.8	A <sub>1</sub>	184.78	0.493
1307.5	A'	85.81	0.384	1345.9	B <sub>2</sub>	41.32	0.110
1317.0	A'	209.60	0.938	1352.8	A <sub>1</sub>	69.97	0.187
1320.3	A'	93.65	0.419	1388.9	A <sub>1</sub>	43.31	0.116
1334.5	A'	107.22	0.480	1511.3	A <sub>1</sub>	45.99	0.123
1347.5	A'	25.35	0.113	1540.9	B <sub>2</sub>	202.38	0.540
1354.1	A'	42.50	0.190	1552.6	A <sub>1</sub>	52.30	0.140
1375.9	A'	22.59	0.101	1556.2	B <sub>2</sub>	44.17	0.118
1387.8	A'	49.18	0.220	1572.0	B <sub>2</sub>	93.62	0.250
1393.7	A'	50.79	0.227	1577.9	A <sub>1</sub>	327.63	0.874
1395.9	A'	22.64	0.101	1582.4	B <sub>2</sub>	112.68	0.301
1399.0	A'	22.44	0.100	1587.4	A <sub>1</sub>	99.66	0.266
1444.6	A'	23.33	0.104	1596.5	A <sub>1</sub>	113.93	0.304
1456.1	A'	40.47	0.181	1606.8	B <sub>2</sub>	63.94	0.171
1465.6	A'	78.15	0.350				
1474.2	A'	23.03	0.103				
1485.8	A'	34.89	0.156				
1504.8	A'	48.40	0.217				
1512.9	A'	145.30	0.650				
1527.9	A'	22.60	0.101				
1544.2	A'	46.45	0.208				
1550.7	A'	223.51	1.00				
1566.5	A'	51.87	0.232				
1576.0	A'	196.49	0.879				
1583.9	A'	34.53	0.155				
1587.0	A'	45.68	0.204				
1590.0	A'	192.43	0.861				
1593.2	A'	26.48	0.118				
1598.2	A'	33.03	0.148				
1606.9	A'	54.35	0.243				
2854.1	A'	2.91	0.013	2876.3	A <sub>1</sub>	0.30	0.001
2866.4	A''	0.27	0.001	2897.0	B <sub>1</sub>	1.01	0.003
3048.2	A'	14.74	0.066	3056.7	A <sub>1</sub>	4.55	0.012
3054.6	A'	5.74	0.026	3057.6	B <sub>2</sub>	1.98	0.005
3055.9	A'	4.03	0.018	3057.7	A <sub>1</sub>	5.55	0.015
3056.7	A'	13.75	0.062	3058.7	B <sub>2</sub>	14.24	0.038
3058.0	A'	7.49	0.033	3058.9	A <sub>1</sub>	1.24	0.003
3059.5	A'	2.79	0.013	3059.9	B <sub>2</sub>	1.95	0.005

Table 7 (Continued)

1-Hydrocircumcoronene				3-Hydrocircumcoronene			
$\tilde{\nu}$ (cm <sup>-1</sup> )	Symmetry	Intensity (km/mol)	$I_{\text{rel}}$	$\tilde{\nu}$ (cm <sup>-1</sup> )	Symmetry	Intensity (km/mol)	$I_{\text{rel}}$
3060.3	A'	3.91	0.018	3060.1	A <sub>1</sub>	9.91	0.026
3060.7	A'	5.30	0.024	3061.0	B <sub>2</sub>	4.34	0.012
3061.7	A'	4.56	0.020	3061.3	A <sub>1</sub>	1.38	0.004
3063.1	A'	0.69	0.003	3062.0	B <sub>2</sub>	4.02	0.011
3077.7	A'	14.93	0.067	3077.2	B <sub>2</sub>	8.38	0.022
3078.1	A'	47.82	0.214	3077.3	A <sub>1</sub>	37.56	0.100
3078.3	A'	53.00	0.237	3078.9	B <sub>2</sub>	0.25	0.001
3079.0	A'	37.63	0.168	3079.0	A <sub>1</sub>	24.30	0.065
3080.8	A'	33.37	0.149	3079.3	B <sub>2</sub>	96.88	0.258
				3079.5	A <sub>1</sub>	29.81	0.080

<sup>a</sup> The data for  $\tilde{\nu} < 2000$  cm<sup>-1</sup> have been truncated at the 10% level. The complete data are tabulated at <http://ccf.arc.nasa.gov/~cbausch/closed-shell.data>.

#### 4.1. The 1600 cm<sup>-1</sup> (6.2 μm) region

Consistent with the behavior of PAH radical cations reported previously [27,39–55], the aromatic CC stretching modes that fall near 1600

cm<sup>-1</sup>, close to the prominent 6.2–6.3 μm interstellar feature, are strongly enhanced in the closed-shell cations compared with the neutral species. In fact, in the spectra of the closed-shell species, this is consistently the strongest band in

Table 8

Calculated frequencies, symmetries, and intensities for the infrared active modes of neutral circumcoronene, C<sub>54</sub>H<sub>18</sub>, and the circumcoronene radical cation, C<sub>54</sub>H<sub>18</sub><sup>+</sup><sup>a</sup>

C <sub>54</sub> H <sub>18</sub>				C <sub>54</sub> H <sub>18</sub> <sup>+</sup>			
$\tilde{\nu}$ (cm <sup>-1</sup> )	Symmetry	Intensity (km/mol)	$I_{\text{rel}}$	$\tilde{\nu}$ (cm <sup>-1</sup> )	Symmetry	Intensity (km/mol)	$I_{\text{rel}}$
782.0	B <sub>3u</sub>	43.30	0.188	919.0	A <sub>u</sub>	216.85	0.226
904.1	B <sub>3u</sub>	220.23	0.954	1246.1	B <sub>u</sub>	112.78	0.118
1286.5	B <sub>1u</sub>	34.37	0.149	1256.9	B <sub>u</sub>	350.64	0.366
1286.6	B <sub>2u</sub>	34.69	0.150	1314.8	B <sub>u</sub>	286.99	0.300
1607.9	B <sub>2u</sub>	26.17	0.113	1351.1	B <sub>u</sub>	164.05	0.171
1608.3	B <sub>1u</sub>	26.09	0.113	1483.6	B <sub>u</sub>	232.83	0.243
				1493.4	B <sub>u</sub>	100.50	0.105
				1570.0	B <sub>u</sub>	141.43	0.148
				1571.2	B <sub>u</sub>	958.13	1.00
3041.8	B <sub>2u</sub>	0.52	0.002	3058.4	B <sub>u</sub>	9.19	0.010
3042.0	B <sub>1u</sub>	0.50	0.002	3059.3	B <sub>u</sub>	11.71	0.012
3045.5	B <sub>1u</sub>	56.58	0.245	3060.4	B <sub>u</sub>	20.79	0.022
3046.0	B <sub>2u</sub>	51.91	0.225	3062.5	B <sub>u</sub>	11.45	0.012
3047.0	B <sub>1u</sub>	2.43	0.011	3063.3	B <sub>u</sub>	9.61	0.010
3062.8	B <sub>2u</sub>	5.31	0.023	3079.8	B <sub>u</sub>	34.87	0.036
3063.4	B <sub>1u</sub>	229.17	0.993	3080.5	B <sub>u</sub>	81.22	0.085
3063.7	B <sub>2u</sub>	230.88	1.00	3080.7	B <sub>u</sub>	106.91	0.112

<sup>a</sup> The data for  $\tilde{\nu} < 2000$  cm<sup>-1</sup> have been truncated at the 10% level. The complete data are tabulated at <http://ccf.arc.nasa.gov/~cbausch/closed-shell.data>.

the spectrum. Of further interest, these features consistently fall at higher frequencies in the closed PAH structures than in the corresponding open-shell species. For example, for circumcoronene (Fig. 9 and Table 8), the most prominent band of the closed-shell neutral species falls at  $1608\text{ cm}^{-1}$  ( $6.219\text{ }\mu\text{m}$ ), while that of the radical cation falls at  $1572\text{ cm}^{-1}$  ( $6.361\text{ }\mu\text{m}$ ). Coronene also exhibits such a trend (neutral,  $1602\text{ cm}^{-1}$ ,  $6.242\text{ }\mu\text{m}$ ; radical cation,  $1554\text{ cm}^{-1}$ ,  $6.435\text{ }\mu\text{m}$ ) [27,40,44]. Although this general trend holds for both the  $C_{\text{odd}}$  and protonated PAH cations considered here, the corresponding vibration falls between  $1590$  and  $1580\text{ cm}^{-1}$  ( $6.29$  and  $6.33\text{ }\mu\text{m}$ ), still somewhat red-shifted from the band position in the parent neutral. While this falls in the red wing of the canonical  $1610\text{ cm}^{-1}$  ( $6.2\text{ }\mu\text{m}$ ) interstellar feature, it is close to the newly discovered  $1590\text{ cm}^{-1}$  ( $6.29\text{ }\mu\text{m}$ ) emission component recently resolved in the high-resolution spectra of a number of objects by the ISO satellite [65]. Overall, given the prominence of the features in this region in the spectra of the closed-shell PAH cations, if a significant population of such species is indeed present in the interstellar medium, they would certainly be expected to dominate the emission at this position.

#### 4.2. The $1500\text{--}1100\text{ cm}^{-1}$ ( $6.7\text{--}9\text{ }\mu\text{m}$ ) region

In the interstellar spectrum, this region is dominated by the strong, broad  $7.7\text{ }\mu\text{m}$  emission envelope and its prominent shoulder near  $8.6\text{ }\mu\text{m}$ . Careful observations [66] have shown that this band is actually a composite of a number of overlapping features dominated by two components falling near  $7.6$  and  $7.8\text{ }\mu\text{m}$ . This spectral region is diagnostic of aromatic CC stretching and CH in-plane bending motions in PAHs. Previous studies of PAH radical cations have established that these modes are strongly enhanced by ionization [27,39–55] and, not surprisingly, the results already presented confirm that this effect also holds for closed-shell cations. Unlike the consistent behavior of the bands in the  $1600\text{ cm}^{-1}$  region already discussed, the direction of the ionization shift experienced by the PAH bands in this range is less predictable. For example, in the

circumcoronene radical cation, the most prominent band in this region falls at  $1256\text{ cm}^{-1}$  ( $7.962\text{ }\mu\text{m}$ ), red-shifted by  $30\text{ cm}^{-1}$  from its position in neutral circumcoronene ( $1286\text{ cm}^{-1}$ ,  $7.776\text{ }\mu\text{m}$ ; see Table 8). Compare this with coronene, where the most prominent band of the radical cation in this region is blue-shifted by  $38\text{ cm}^{-1}$  (cation,  $1350\text{ cm}^{-1}$ ,  $7.407\text{ }\mu\text{m}$ ; neutral,  $1312\text{ cm}^{-1}$ ,  $7.622\text{ }\mu\text{m}$ ) [40,44]. Nonetheless, there is an underlying consistency with the interstellar emission spectrum. In each case, the dominant bands tend to fall within the envelope of the interstellar  $7.6\text{ }\mu\text{m}$  ( $1315\text{ cm}^{-1}$ ) component that dominates the  $7.7\text{ }\mu\text{m}$  emission envelope in HII regions and reflection nebula [66]. Indeed, inspection of the tables show that, in general, for both the  $C_{\text{odd}}$ -PAH and HPAH<sup>+</sup> cations considered here, the dominant features in this region typically fall between  $1350$  and  $1314\text{ cm}^{-1}$  ( $7.41$  and  $7.61\text{ }\mu\text{m}$ ), most consistent with the position of the interstellar  $7.6\text{ }\mu\text{m}$  component. The detailed origin of the strong  $7.8\text{ }\mu\text{m}$  component therefore remains unclear.

In addition to the aromatic modes that fall in this region, the HPAH<sup>+</sup> species have an additional, unique contribution in this region of the spectrum. The aliphatic  $\text{CH}_2$  deformation modes of these species are expected to fall in the mid- $1400\text{ cm}^{-1}$  ( $\sim 7\text{ }\mu\text{m}$ ) range [67]. Indeed, the greater spectral complexity that is observed throughout this region in the protonated PAH cations is no doubt partially attributable to the contributions of the aliphatic modes. As with the aromatic modes in this region, the aliphatic deformation modes are enhanced by ionization and are actually more intense than the strong aliphatic CH stretching bands (see Tables 4–7) that dominate the spectra of neutral hydrogenated PAHs. However, as already noted, these modes mix with the aromatic CC stretching and CH in-plane bending modes to such a degree that it is not possible to distinguish between ‘aliphatic’ and ‘aromatic’ modes in this region.

A final, consistent aspect of the spectra of these species with the interstellar emission spectra is the presence of a prominent band in the  $1214\text{--}1140\text{ cm}^{-1}$  ( $8.24\text{--}8.77\text{ }\mu\text{m}$ ) range that corresponds most closely to the interstellar  $8.6\text{ }\mu\text{m}$  ( $1165\text{ cm}^{-1}$ ) component of the interstellar emission

spectrum. For the closed-shell cations considered here, the intensities of these bands relative to the dominant  $1300\text{ cm}^{-1}$  bands also echo that of the interstellar emission.

#### 4.3. The $3200\text{--}2800\text{ cm}^{-1}$ ( $3.1\text{--}3.6\text{ }\mu\text{m}$ ) region

The other region in which closed-shell cations potentially impact the interstellar emission spectrum is in the CH stretching region between  $3200$  and  $2800\text{ cm}^{-1}$  ( $3.1$  and  $3.6\text{ }\mu\text{m}$ ). While all of the species considered here would certainly contribute to the well-known  $3.3\text{ }\mu\text{m}$  emission band (aromatic CH stretching modes), of particular interest is the contribution of the HPAH<sup>+</sup> species to the variable emission complex that falls on the red wing of the aromatic feature between  $\sim 3.4$  and  $3.5\text{ }\mu\text{m}$ . This range is diagnostic of aliphatic CH stretching modes and, as expected, inspection of Figs. 6–9 shows that protonation is accompanied by the appearance of a feature that is attributable to these modes. In each of the HPAH<sup>+</sup> considered here, the aliphatic CH stretching region displays a pair of bands that are typically separated by  $5\text{--}20\text{ cm}^{-1}$  and centered near  $2860\text{ cm}^{-1}$  ( $3.5\text{ }\mu\text{m}$ ). The distribution of intensity between these bands is variable, but in all but one case it is the lower frequency band that dominates the pair (see Tables 4–7).

The dominance of the  $3.3\text{ }\mu\text{m}$  aromatic CH stretching feature over the aliphatic CH stretching feature in the typical interstellar emission spectrum, despite the markedly greater intrinsic strength of the latter modes, indicates that the interstellar emitting population is predominantly aromatic with only a modest degree of aliphatic character. Given the great abundance of hydrogen in the interstellar medium and the inherent favorability of the closed-shell HPAH<sup>+</sup> species, it is tempting to posit that simple protonation across the PAH cation population might contribute sufficient aliphatic character to account for the interstellar  $3.4\text{--}3.5\text{ }\mu\text{m}$  emission. This idea is, however, not borne out by the data presented in this article. As already mentioned, the protonated species discussed in Section 3.2 consistently display only a single noteworthy feature near  $2860\text{ cm}^{-1}$  ( $3.50\text{ }\mu\text{m}$ ). Thus, while such species likely contribute to the interstellar emission in this region, they cannot

in-and-of-themselves explain the spectral complexity that is observed in that spectrum. Instead, that complexity implies a modest subpopulation of more highly hydrogenated species ( $\text{H}_n\text{PAHs}$  and/or their associated ions) [22].

#### 4.4. The $900\text{--}700\text{ cm}^{-1}$ ( $11\text{--}14\text{ }\mu\text{m}$ ) region

Finally, it is interesting to note that, although there are twice as many doubly-adjacent CH groups as non-adjacent CH groups in  $\text{C}_{59}\text{H}_{19}^+$ , the circumcoronene radical cation, and the hydrogenated circumcoronene cations, the  $900\text{--}700\text{ cm}^{-1}$  ( $11\text{--}14\text{ }\mu\text{m}$ ) CH out-of-plane bending region is dominated by only one band. That band consistently falls near  $930\text{--}920\text{ cm}^{-1}$  ( $10.75\text{--}10.87\text{ }\mu\text{m}$ ), close to the position of non-adjacent CH groups on open shell PAH cations that have previously been proposed as a tracer of the ionized interstellar PAH component [68].

## 5. Conclusions

Prompted by recent experimental studies that indicate such species may play an important role in the interstellar medium, we have carried out B3LYP/4/31G calculations to determine the harmonic frequencies and intensities for a variety of closed-shell PAH cations. The set of species considered extends over a wide range of molecular sizes and includes both  $\text{C}_{\text{odd}}$  PAH cations — fully benzenoid species composed of an odd number of carbon atoms — and protonated PAHs.

Overall, the spectra of closed-shell PAH cations are consistent with previously reported theoretical and experimental spectra of PAH radical cations, and with the global pattern of band positions and intensities in the interstellar emission spectrum. The spectra do, however, display some distinctive features that distinguish them from the PAH species considered previously. The  $\text{C}_{\text{odd}}$  PAH cation spectra, for example, display a notably weaker dependence on molecular size than is typical of either the protonated PAHs considered here or of the PAH radical cations that can be found in the literature. Furthermore, the spectra of these species are dominated by several strong features in the

1600–1100  $\text{cm}^{-1}$  region, the strongest of which is consistently the highest frequency band falling near 1600  $\text{cm}^{-1}$ . Thus, if these species are, indeed, common in the interstellar medium, they would be expected to make a disproportionate contribution to the 6.2  $\mu\text{m}$  infrared emission band.

The protonated PAHs tend to display a greater degree of spectral complexity compared with their parent radical cation. This is due both to a lowering of the symmetry of the cation as well as to the contributions of the characteristic aliphatic modes of the associated  $\text{CH}_2$  group.

Finally, for both classes of closed-shell PAH cations, increasing molecular size is found to be accompanied by a strong increase in the intensity of the aromatic CH stretching features. Analysis of the Mulliken populations indicates that this is a consequence of the decrease in charge density within the molecule as the positive charge is smeared over a larger and larger molecular skeleton. Consequently, the character of these modes, which are, in general, strongly suppressed in PAH cations, gradually approaches the dominant character of the analogous modes in neutral PAHs. In contrast, the aliphatic CH stretching modes of the protonated PAHs are increasingly suppressed with increasing molecular size. The origin of this effect is not yet clearly understood and will require further study.

## Acknowledgements

Two of the authors (D.M.H., L.J.A.) would like to thank the editors of this issue for contributing their time and effort to organize this special journal edition. We also gratefully acknowledge support under NASA's Long Term Space Astrophysics Program (Grant 399-20-01).

## References

- [1] F.C. Gillett, W.J. Forrest, K.M. Merrill, *Astrophys. J.* 183 (1973) 87.
- [2] R.W. Russell, B.T. Soifer, S.P. Willner, *Astrophys. J.* 217 (1977) L149.
- [3] D.K. Aitken, in: C.G. Wynn-Williams, D.P. Cruikshank (Eds.), *Infrared Astronomy*, Reidel, Dordrecht, 1981, p. 207.
- [4] S.P. Willner, in: M.F. Kessler, J.P. Phillips (Eds.), *Galactic and Extragalactic Infrared Spectroscopy*, Reidel, Dordrecht, 1984, p. 37.
- [5] M.M. Phillips, D.K. Aitken, P.F. Roche, *Mon. Not. R. Astron. Soc.* 207 (1984) 25.
- [6] T.R. Geballe, A.G.G.M. Tielens, S. Kwok, B.J. Hrivnak, *Astrophys. J.* 387 (1992) L89.
- [7] P.R. Roelfsema, et al., *Astron. Astrophys.* 315 (1996) L289.
- [8] R.J. Laureijs, et al., *Astron. Astrophys.* 315 (1996) L313.
- [9] T. Onaka, I. Yamamura, T. Tanabe, T.L. Roellig, L. Yuen, *Pub. Astron. Soc. Jpn.* 48 (1996) L59.
- [10] K. Matilla, et al., *Astron. Astrophys.* 315 (1996) L353.
- [11] G.C. Sloan, J.D. Bregman, T.R. Geballe, L.J. Allamandola, C.E. Woodward, *Astrophys. J.* 474 (1997) 735.
- [12] A. Leger, J.L. Puget, *Astron. Astrophys.* 137 (1984) L5.
- [13] L.J. Allamandola, A.G.G.M. Tielens, J.R. Barker, *Astrophys. J.* 290 (1985) L25.
- [14] K. Sellgren, *Astrophys. J.* 277 (1984) 627.
- [15] M. Cohen, A.G.G.M. Tielens, L.J. Allamandola, *Astrophys. J.* 299 (1985) L93.
- [16] M. Cohen, L.J. Allamandola, A.G.G.M. Tielens, J. Bregman, J.P. Simpson, F.C. Witteborn, D. Wooden, D. Rank, *Astrophys. J.* 302 (1986) 737.
- [17] M. Cohen, A.G.G.M. Tielens, J. Bregman, F.C. Witteborn, D. Rank, L.J. Allamandola, D. Wooden, M. DeMuizon, *Astrophys. J.* 341 (1989) 246.
- [18] W. Schutte, A.G.G.M. Tielens, L.J. Allamandola, *Astrophys. J.* 415 (1993) 397.
- [19] E.L.O. Bakes, A.G.G.M. Tielens, *Astrophys. J.* 427 (1994) 822.
- [20] F. Salama, E.L.O. Bakes, L.J. Allamandola, A.G.G.M. Tielens, *Astrophys. J.* 458 (1996) 621.
- [21] H.W. Jochims, E. Ruhl, H. Baumgartel, S. Tobita, S. Leach, *Astrophys. J.* 420 (1994) 307.
- [22] M.P. Bernstein, S.A. Sandford, L.J. Allamandola, *Astrophys. J.* 472 (1996) L127.
- [23] V. LePage, Y. Keheyian, V. Bierbaum, T. Snow, *J. Am. Chem. Soc.* 119 (1997) 8373.
- [24] T. Snow, V. Le Page, Y. Keheyian, V. Bierbaum, *Nature* 391 (1997) 259.
- [25] E.L.O. Bakes, A.G.G.M. Tielens, *Astrophys. J.* 499 (1998) 258.
- [26] L.J. Allamandola, A.G.G.M. Tielens, J.R. Barker, *Astrophys. J. Suppl. Ser.* 71 (1989) 733.
- [27] D.J. DeFrees, M.D. Miller, in: L.J. Allamandola, A.G.G.M. Tielens (Eds.), *Interstellar Dust: Contributed Papers*, NASA CP 3036, 1989, p. 173.
- [28] J.D. Brenner, J.R. Barker, *Astrophys. J.* 388 (1992) L39.
- [29] F. Pauzat, D. Talbi, M.D. Miller, D.J. DeFrees, Y. Ellinger, *J. Phys. Chem.* 96 (1992) 7882.
- [30] D.J. DeFrees, M.D. Miller, D. Talbi, F. Pauzat, Y.J. Ellinger, *Astrophys. J.* 408 (1993) 530.
- [31] J. Szczepanski, M. Vala, *Nature* 363 (1993) 699.
- [32] F. Salama, C. Joblin, L.J. Allamandola, *J. Chem. Phys.* 101 (1994) 10252.

- [33] D. Hudgins, S.A. Sandford, L.J. Allamandola, *J. Phys. Chem.* 98 (1994) 4243.
- [34] S. Schlemmer, D.J. Cook, J.A. Harrison, B. Wurfel, W. Chapman, R.J. Saykally, *Science* 265 (1994) 1686.
- [35] S.R. Langhoff, *J. Phys. Chem.* 100 (1996) 2819.
- [36] C.W. Bauschlicher, Jr, S.R. Langhoff, *Spectrochim. Acta A* 53 (1997) 1225.
- [37] D.J. Cook, R.J. Saykally, *Astrophys. J.* 493 (1998) 793.
- [38] H. Piest, G. von Helden, G. Meijer, *Astrophys. J.* 520 (1999) L75.
- [39] D.M. Hudgins, S.A. Sandford, L.J. Allamandola, *J. Phys. Chem.* 98 (1994) 4243.
- [40] D.M. Hudgins, L.J. Allamandola, *J. Phys. Chem.* 99 (1995) 3033.
- [41] D.M. Hudgins, L.J. Allamandola, *J. Phys. Chem.* 99 (1995) 8978.
- [42] D.M. Hudgins, L.J. Allamandola, *J. Phys. Chem. A* 101 (1997) 3472.
- [43] D.M. Hudgins, S.A. Sandford, *J. Phys. Chem. A* 102 (1998) 329.
- [44] D.M. Hudgins, S.A. Sandford, *J. Phys. Chem. A* 102 (1998) 344.
- [45] D.M. Hudgins, S.A. Sandford, *J. Phys. Chem. A* 102 (1998) 353.
- [46] D.M. Hudgins, L.J. Allamandola, C.W. Bauschlicher, Jr, J. Fetzer, *J. Phys. Chem. A* 104 (2000) 3655.
- [47] J. Szczepanski, M. Vala, D. Talbi, O. Parisel, Y. Ellinger, *J. Chem. Phys.* 98 (1993) 4494.
- [48] J. Szczepanski, C. Chapo, M. Vala, *Chem. Phys. Lett.* 205 (1993) 434.
- [49] J. Szczepanski, M. Vala, *Astrophys. J.* 414 (1993) 179.
- [50] M. Vala, J. Szczepanski, F. Pauzat, O. Parisel, D. Talbi, Y. Ellinger, *J. Phys. Chem.* 98 (1994) 9187.
- [51] J. Szczepanski, C. Wehlberg, M. Vala, *Chem. Phys. Lett.* 232 (1995) 221.
- [52] J. Szczepanski, J. Drawdy, C. Wehlburg, M. Vala, *Chem. Phys. Lett.* 245 (1995) 539.
- [53] C.W. Bauschlicher, S.R. Langhoff, S.A. Sandford, D.M. Hudgins, *J. Phys. Chem. A* 101 (1997) 2414.
- [54] S.R. Langhoff, C.W. Bauschlicher, Jr, D.M. Hudgins, S.A. Sandford, L.J. Allamandola, *J. Phys. Chem. A* 102 (1998) 1632.
- [55] C.W. Bauschlicher, Jr, D.M. Hudgins, L.J. Allamandola, *Theor. Chem. Acc.* 103 (1999) 154.
- [56] D.M. Hudgins, L.J. Allamandola, *Astrophys. J.* 513 (1999) L69.
- [57] R.E. Stratmann, G.E. Scuseria, M.J. Frisch, *Chem. Phys. Lett.* 257 (1996) 213.
- [58] P.J. Stephens, F.J. Devlin, C.F. Chabalowski, M.J. Frisch, *J. Phys. Chem.* 98 (1994) 11623.
- [59] A.D. Becke, *J. Chem. Phys.* 98 (1993) 5648.
- [60] M.J. Frisch, J.A. Pople, J.S. Binkley, *J. Chem. Phys.* 80 (1984) 3265.
- [61] M.J. Frisch, G.W. Trucks, H.B. Schlegel, G.E. Scuseria, M.A. Robb, J.R. Cheeseman, V.G. Zakrzewski, J.A. Montgomery, Jr., R.E. Stratmann, J.C. Burant, S. Dapprich, J.M. Millam, A.D. Daniels, K.N. Kudin, M.C. Strain, O. Farkas, J. Tomasi, V. Barone, M. Cossi, R. Cammi, B. Mennucci, C. Pomelli, C. Adamo, S. Clifford, J. Ochterski, G.A. Petersson, P.Y. Ayala, Q. Cui, K. Morokuma, D.K. Malick, A.D. Rabuck, K. Raghavachari, J.B. Foresman, J. Cioslowski, J.V. Ortiz, A.G. Baboul, B.B. Stefanov, G. Liu, A. Liashenko, P. Piskorz, I. Komaromi, R. Gomperts, R.L. Martin, D.J. Fox, T. Keith, M.A. Al-Laham, C.Y. Peng, A. Nanayakkara, C. Gonzalez, M. Challacombe, P.M.W. Gill, B. Johnson, W. Chen, M.W. Wong, J.L. Andres, C. Gonzalez, M. Head-Gordon, E.S. Replogle, J.A. Pople, *GAUSSIAN 98*, Revision A.7, Gaussian, Inc., Pittsburgh, PA, 1998.
- [62] P. Weilmunster, A. Keller, K.-H. Homann, *Comb. Flame* 116 (1998) 62.
- [63] M. Franklach, E.D. Feigelson, *Astrophys. J.* 341 (1989) 372.
- [64] I. Cherchneff, J.R. Barker, A.G.G.M. Tielens, *Astrophys. J.* 401 (1992) 269.
- [65] E. Peeters, S. Hony, C. Van Kerckhoven, A.G.G.M. Tielens, L.J. Allamandola, D.M. Hudgins, *Astron. Astrophys.* (in preparation).
- [66] J.D. Bregman, in: L.J. Allamandola, A.G.G.M. Tielens (Eds.), *Interstellar Dust*, Kluwer, Dordrecht, 1989, p. 109.
- [67] L.J. Bellamy, *The Infrared Spectra of Complex Organic Molecules*, Wiley, New York, 1958.
- [68] D.M. Hudgins, L.J. Allamandola, *Astrophys. J.* 516 (1999) L41.